© 2022. Published by The Company of Biologists Ltd | Development (2022) 149, dev200892. doi:10.1242/dev.200892

RESEARCH ARTICLE

The functional specificity of ERECTA-family receptors in *Arabidopsis* stomatal development is ensured by molecular chaperones in the endoplasmic reticulum

Ke-Zhen Yang[1,*], Chao-Ran Zuo[1,2,*], Ya-Jun Leng[3,*], Jun-Ling Yue[1,2], Hui-Chao Liu[1,2], Zhi-Bin Fan[1,2], Xue-Yi Xue[4], Juan Dong[5,6], Li-Qun Chen[3,‡] and Jie Le[1,2,‡]

ABSTRACT

Stomata are epidermal pores that control gas exchange between plants and the atmosphere. In *Arabidopsis*, the ERECTA family (ERECTAf) receptors, including ERECTA, ERECTA-LIKE 1 (ERL1) and ERL2, redundantly play pivotal roles in enforcing the 'one-cell-spacing' rule. Accumulating evidence has demonstrated that the functional specificities of receptors are likely associated with their differential subcellular dynamics. The endoplasmic reticulum (ER)-resident chaperone complex SDF2-ERdj3B-BiP functions in many aspects of plant development. We employed pharmacological treatments combined with cell biological and biochemical approaches to demonstrate that the abundance of ERECTA was reduced in the *erdj3b-1* mutant, but the localization and dynamics of ERECTA were not noticeably affected. By contrast, the *erdj3b* mutation caused the retention of ERL1/ERL2 in the ER. Furthermore, we found that the function of SDF2-ERdj3B-BiP is implicated with the distinct roles of ERECTAf receptors. Our findings establish that the ERECTAf receptor-mediated signaling in stomatal development is ensured by the activities of the ER quality control system, which preferentially maintains the protein abundance of ERECTA and proper subcellular dynamics of ERL1/ERL2, prior to the receptors reaching their destination – the plasma membrane – to execute their functions.

KEY WORDS: *Arabidopsis*, Stomatal development, ERECTA receptor, SDF2-ERdj3B-BiP, Molecular chaperone, Endoplasmic reticulum quality control

INTRODUCTION

Stomata are epidermal pores that play important roles in gas exchange between plants and the atmosphere. In *Arabidopsis*, a subpopulation of protodermal cells adopts the stomatal lineage identity to become meristemoid mother cells (MMCs). An MMC undergoes asymmetric cell division to create two daughter cells with distinct identity: a smaller meristemoid and a larger stomatal lineage ground cell (SLGC). Both meristemoids and SLGCs have the potential to further divide asymmetrically, but each has a different cell-fate trajectory. Meristemoids differentiate into guard mother cells (GMCs) and eventually produce a pair of kidney-shaped guard cells (GCs) after GMC symmetric division. SLGCs ultimately become puzzle-shaped pavement cells in the epidermis (Nadeau and Sack, 2002; Dong and Bergmann, 2010; Torii, 2012).

Stomatal formation and pattern comply with the 'one-cell-spacing' rule, by which each stoma is spaced out by at least one pavement cell. It was believed that short-distance signaling mediated by peptide ligand-receptor signal transduction specifies cell-to-cell communication during stomatal pattern formation. The identified key components include secretory peptides from the epidermal patterning factor (EPF)/EPF-like (EPFL) protein family (Hunt and Gray, 2009; Sugano et al., 2010), the leucine-rich repeat (LRR) receptor protein TOO MANY MOUTHS (TMM) (Nadeau and Sack, 2002) and the ERECTA family (ERECTAf) and somatic embryogenesis receptor-like kinase (SERK) family receptors (Meng et al., 2015; Shpak et al., 2005). Three ERECTAf receptors, including ERECTA, ERECTA-LIKE1 (ERL1) and ERL2, redundantly govern the initial decision of stomatal lineage in the epidermis. The fine-scale genetic analyses revealed that individual members may contribute differently to stomatal division and differentiation. Loss of function of all three ERECTAf genes was found to cause large stomatal clustering (Shpak et al., 2005). The single mutation of *erecta* resulted in excessive stomatal precursor-like cells (PrCs) that failed to differentiate into mature stomata. With an additional *erl2* mutation in *erecta erl2* double mutants, the formation of excessive PrCs was enhanced. By contrast, additional mutation of *erl1* promoted the differentiation of arrested PrCs into stomata in *erecta* and *erecta erl2* double mutants (Shpak et al., 2005). Thus, although the collective function of the ERECTA family is to suppress stomatal initiation, individual members contribute differently to different aspects of stomatal division and differentiation (Shpak et al., 2005).

In eukaryotic cells, secretory proteins, including cell-surface receptors, are synthesized by the endoplasmic reticulum (ER)-bound ribosomes. Nascent proteins are then translocated into the ER lumen where carbohydrates are added primarily to newly synthesized, unfolded proteins. As the above processes are error prone, eukaryotic cells have an ER quality control (ERQC) system that monitors protein conformation and eliminates terminally misfolded polypeptides through ER-associated degradation (ERAD) or autophagic degradation (Strasser, 2018).

[1]Key Laboratory of Plant Molecular Physiology, CAS Center for Excellence in Molecular Plant Sciences, Institute of Botany, Chinese Academy of Sciences, Beijing 100093, China. [2]University of Chinese Academy of Sciences, Beijing 100049, China. [3]State Key Laboratory of Plant Physiology and Biochemistry, College of Biological Sciences, China Agricultural University, Beijing 100193, China. [4]Department of Plant Biology, University of Illinois at Urbana-Champaign, Urbana, IL 61801, USA. [5]Waksman Institute of Microbiology, Rutgers, The State University of New Jersey, Piscataway, NJ 08854, USA. [6]Department of Plant Biology, Rutgers, The State University of New Jersey, New Brunswick, NJ 08901, USA.
*These authors contributed equally to this work

‡Authors for correspondence (chenliqun@cau.edu.cn; lejie@ibcas.ac.cn)

K.-Z.Y., 0000-0002-6775-8946; Y.-J.L., 0000-0002-8698-210X; J.D., 0000-0002-3089-3167; L.-Q.C., 0000-0002-8179-6172; J.L., 0000-0001-8854-3031

Handling Editor: Ykä Helariutta
Received 3 May 2022; Accepted 23 August 2022

Development (2022) 149, dev200892. doi:10.1242/dev.200892

The maintenance of protein homeostasis of cell-surface receptors involves ERQC events in plants. For example, misfolded growth receptor BRASSINOSTEROID INSENSTITIVE 1 (BRI1) was shown to be retained in the ER and degraded by a glycan-dependent ERAD process (Hong et al., 2012). Limited evidence has already shown that VAP-RELATED SUPPRESSOR OF TMM (VST, PapD-like superfamily protein) proteins facilitate ERECTAf signal transduction, possibly through an interaction between VST1 and the ER-localized proteins SOYBEAN GENE REGULATED BY COLD-2 (SRC2) and SYNAPTOTAGMIN A (SYT1) (Ho et al., 2016). Also, it has recently been shown that EPFL9/STOMAGEN triggers the retention of ERL1 in the ER (Qi et al., 2020).

The ER-resident SDF2-ERdj3-BiP chaperone complex plays an important role in protein folding, maturation and degradation in ERQC (Buchberger et al., 2010; Strasser, 2018). In *Arabidopsis*, luminal binding proteins (BiPs) have three homologs in the genome (*BIP1*, *BIP2* and *BIP3*). No phenotype was found in single mutants of these genes under normal conditions, but higher-order mutants displayed a pollen development defect (Yamamoto et al., 2008; Maruyama et al., 2014a,b). There are two ERDJ3 homologs in *Arabidopsis*, including *ERDJ3A/TMS1* and *ERDJ3B*. *ERDJ3A* is mainly expressed in pollen, and its mutation in a L*er* background led to a pollen defect at high temperatures (Yang et al., 2009). By contrast, *ERDJ3B* is widely expressed in all organs, but no obvious phenotype was found in the *erdj3b* single mutant. Recent results showed that *ERDJ3B* was involved in anther and ovule development at high temperatures (Yamamoto et al., 2020; Leng et al., 2022). However, whether the SDF2-ERdj3B-BiP chaperone complex is required for stomatal development by regulating ERECTAf receptors has not been experimentally examined.

Here, we employed pharmacological treatments combined with genetic, cell biological and biochemical strategies to demonstrate that, among the stomatal receptors, individual ERECTAf receptors are distinctly modulated by the SDF2-ERdj3B-BiP chaperone complex. Despite the ERECTAf receptors having high sequence similarity, the SDF2-ERdj3B-BiP chaperone complex appeared to specifically maintain the protein abundance of ERECTA, while promoting the ER exit and translocation of ERL1/ERL2 to the plasma membrane (PM).

RESULTS

ER stress influences the action of ERECTAf receptors

Protein N-glycosylation is closely linked with protein folding and plays an important role in ERQC (Helenius and Aebi, 2004). Several conserved N-glycosylation motifs have been predicted in the LRR ectodomain of all three ERECTAf receptors (Chakraborty et al., 2019). To assay possible involvement of ERQC in stomatal development, wild-type *Arabidopsis* seedlings were treated with tunicamycin (TM), an inhibitor of N-glycosylation (Olden et al., 1982). At a low concentration (30 ng/ml) of TM, no obvious stomatal phenotype was found (Fig. 1A,B), but treatment with a high concentration (60 ng/ml) induced the formation of stomatal clusters (Fig. 1C), consistent with previous observations (Ho et al., 2016). When higher concentrations of TM (120 ng/ml or 240 ng/ml) were applied, the stomatal clustering phenotype became more severe and unpaired GCs within stomatal clusters appeared (Fig. 1D-F). Thus, TM treatment affects stomatal development in a dosage-dependent manner.

ERECTAf receptors redundantly regulate the initial decision and distribution of the stomatal lineage in the epidermis (Shpak et al., 2005). Likely owing to the redundant function of ERECTA in stomatal patterning control, the stomatal phenotype in *erl1-5 erl2-3* double mutant was normal (Fig. 1G). However, the TM-induced stomatal clustering phenotype in *erl1-5 erl2-3* was more severe than that found in wild-type cotyledons after 60 ng/ml TM treatment (Fig. 1H versus Fig. 1C). For instance, about 37% stomatal units in *erl1-5 erl2-3* consisted of more than four GCs, compared with 10% in the wild type, indicating a redundant function of ERECTA in resistance to TM-induced stomatal clustering (Fig. 1I).

We analyzed the expression level and subcellular localization of fluorescent protein-tagged ERECTAf receptors. *ERECTA:ERECTA-YFP* complemented the stomatal phenotype of the *erecta* mutant *er-105* and predominantly localized at the PM in all epidermal cells (Fig. 1J). After TM treatment for 24 h, no obvious differences in the expression level and subcellular distribution pattern of ERECTA-YFP were found (Fig. 1K). However, a prolonged TM treatment of 48 h resulted in an increase of intracellular ERECTA-YFP fluorescence signals (Fig. 1L,M).

Immunoblotting results confirmed the increase in ERECTA protein levels in TM-treated ERECTA-FLAG transgenic plants (Fig. 1N). However, a large portion of ERECTA-FLAG proteins from the TM-treated plants displayed a faster mobility, which might be due to the increase of newly synthesized proteins with defective protein glycosylation. As *ERECTA-FLAG* expression was driven by the 35S promoter, we examined the transcription of the *ERECTA* gene in non-transgenic wild-type plants. However, no significant change in *ERECTA* transcript levels was found after TM treatment (Fig. S1A). Thus, the enhanced abundance of the ERECTA-FLAG protein in TM-treated plants might be caused by increased protein synthesis or reduced protein degradation. Next, ERECTA-FLAG seedlings were co-treated with TM and cycloheximide (CHX), a protein synthesis inhibitor, or MG-132, a widely used protein degradation inhibitor that can repress the activity of the 26S proteasome. As detected by immunoblotting, the abundance of the ERECTA-FLAG protein was significantly reduced by CHX treatment (Fig. S1I). TM-induced protein accumulation was also abolished by CHX treatment. Inhibition of protein degradation by MG-132 caused an increase in ERECTA-FLAG protein levels. However, the combination of TM and MG-132 treatment conferred a stronger accumulation of ERECTA-FLAG proteins (Fig. S1J). These results indicate that the TM-induced increase of ERECTA protein abundance was mainly caused by the increased protein synthesis instead of reduced degradation. Similarly, the enhanced accumulation of ERL1-FLAG and ERL2-FLAG proteins in TM-treated *ERL1-FLAG* and *ERL2-FLAG* plants was due to increased protein synthesis (Fig. 1T; Fig. S1K-N).

To further analyze the glycosylation status of the ERECTA protein, the enzyme endoglycosidase H (Endo-H), which primarily cleaves N-linked glycans of ER-localized proteins but not the complex glycans of proteins that are transported into the Golgi apparatus and further in the secretory pathway, was used to digest the proteins extracted from *ERECTA-FLAG* transgenic plants (Jin et al., 2007; Nekrasov et al., 2009; Qi et al., 2020). In control plants (DMSO mock treatment), two bands were detected by using anti-FLAG antibodies for immunoblotting after Endo-H digestion, a lower band (N-glycans removed) and an upper band (non-cleaved protein), indicating that the ERECTA protein was partially retained in the ER. However, in TM-treated *ERECTA-FLAG* plants, the upper band could barely be detected after Endo-H digestion, suggesting that TM treatment greatly enhanced the retention of the ERECTA protein in the ER (Fig. 1O; Fig. S1D).

In *ERL1:ERL1-YFP* plants, ERL1-YFP mainly localized at the PM and partially appeared in the endosomes of stomatal precursor

Development (2022) 149, dev200892. doi:10.1242/dev.200892

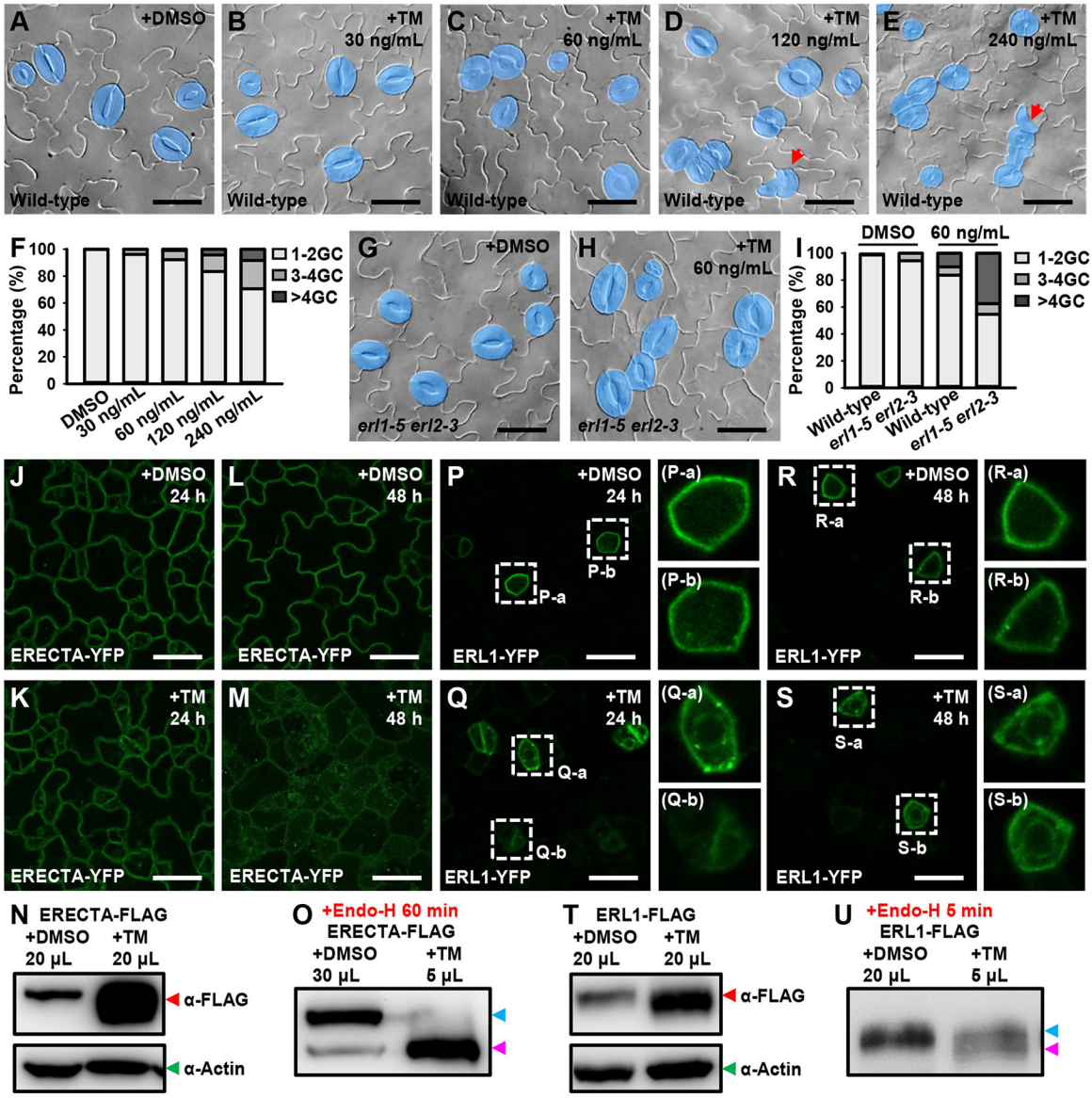

Fig. 1. Response of stomatal development and receptors to TM-induced ER stress. (A-E) DIC images of TM-treated wild-type epidermis. TM at 30 ng/ml had no effect on the stomatal phenotype, whereas 60 ng/ml induced stomatal clusters. TM at 120 ng/ml or 240 ng/ml induced more severe clustering phenotypes. GCs are highlighted by blue color. Red arrows, unpaired guard cells within stomatal clusters. (F) Quantification of stomatal phenotypes after treatment with TM at different concentrations. (G-I) DIC images and quantification of stomatal phenotypes of TM-treated *erl1-5 erl2-3* mutant. *erl1-5 erl2-3* was more sensitive to 60 ng/ml TM treatment than the wild-type. (J-M) Confocal images of *ERECTA:ERECTA-YFP* in epidermal cells. A reduction in PM-localized ERECTA-YFP levels with an increase of intracellular signals was seen after 48 h TM treatment. (N) Immunoblotting analysis indicated an increase in ERECTA-FLAG levels after TM treatment. Top panel, ERECTA-FLAG recognized by anti-FLAG (red arrowhead); lower panel, the loading control of actin detected by anti-actin (green arrowhead). (O) Immunoblotting analysis of ERECTA-FLAG after 60 min digestion with Endo-H, indicating that ERECTA-FLAG extracted from TM-treated plants was sensitive to Endo-H. Upper band, non-cleaved proteins (blue arrowhead); lower band, proteins with N-glycans removed (pink arrowhead). See also Fig. S1D. (P-S) Confocal images of *ERL1:ERL1-YFP* expression in stomatal lineage cells. PM and punctate localization of ERL1-YFP were altered after TM treatment. Images on the right show higher magnifications of the regions indicated by the dotted white boxes. (T) Immunoblotting analysis shows an increase of ERL1-FLAG levels after TM treatment (red arrowhead). (U) Immunoblotting analysis of ERL1-FLAG after a 5 min digestion with Endo-H, indicating that ERL1-FLAG extracted from TM-treated plants is sensitive to Endo-H digestion. See also Fig. S1E. Images are representative of three independent experiments. Scale bars: 20 µm.

cells (Fig. 1P,R) (Qi et al., 2020). Interestingly, unlike ERECTA-YFP, ERL1-YFP showed significant accumulation in the ring-like structure after TM treatment (Fig. 1Q,S). *ERL2:ERL2-YFP* plants exhibited punctate and PM localization of ERL2 in stomatal lineage cells (Ho et al., 2016). Like ERL1-YFP, ERL2-YFP signals also accumulated in a ring-like structure after TM treatment (Fig. S1F,G). Similar to ERECTA-FLAG, both ERL1-FLAG and ERL2-FLAG from TM-treated plants were hypersensitive to Endo-H digestion (Fig. 1U; Fig. S1E,H).

In addition, we examined the effect of TM on YFP-tagged SERK3 and GFP-tagged BRI1, which are PM-localized receptors and have functions in stomatal development (Meng et al., 2015; Kim et al., 2012). However, after 48 h of TM treatment, no obvious changes in the expression level and subcellular localization of SERK3-YFP and BRI1-GFP were found (Fig. S1O-R). Taken together, our results suggest that protein N-glycosylation affects protein biogenesis, subcellular localization and function of ERECTAf receptors in stomatal development.

Development (2022) 149, dev200892. doi:10.1242/dev.200892

Dysfunction of the ER-resident chaperone complex reduces the abundance but not the subcellular dynamics of ERECTA

ERdj3B is the core component of the SDF2-ERdj3B-BiP complex, but none of the three ERECTAf genes showed significant changes in transcript levels in the *erdj3b-1* mutant (Fig. S2). Then, we analyzed the total protein abundance of the ERECTAf receptors in the *erdj3b-1* mutant by using rabbit polyclonal antibodies that recognize all three ERECTAf proteins. The total ERECTAf protein levels were 60% lower in the *erdj3b-1* mutant than those in wild-type plants (Fig. 2A).

To further narrow down whether individual ERECTAf proteins were differentially affected in the *erdj3b-1* mutant, by using the same antibodies, we evaluated the total ERECTAf protein amount in double mutants for different combinations of ERECTAf genes; each mutant would contain the third family member intact in the genome. We found a dramatic reduction of protein abundance in *erdj3b-1 erl1-5 erl2-3*, compared with *erl1-5 erl2-3* (Fig. 2B). By contrast, the total protein amounts in *erdj3b-1 er-105 erl1-5* and *erdj3b-1 er-105 erl2-3* were slightly changed compared with those in *er-105 erl1-5* and *er-105 erl2-3*, respectively (Fig. 2C,D). These results suggested that the lowered total protein levels of ERECTAf receptor proteins in *erdj3b-1* were mainly caused by a decrease in the levels of ERECTA, rather than those of ERL1 or ERL2.

Then, we investigated whether the *erdj3b* mutation affected the subcellular localization of the ERECTAf receptors. ERECTA-YFP (*er-105* complementary) was colocalized with the styryl dye FM4-64 at the PM (Fig. 2E). Consisting with immunoblotting results, the overall fluorescence intensity of ERECTA-YFP in *erdj3b-1* was dramatically reduced, especially at the PM (Fig. 2F). In addition, the reduced expression level of ERECTA-YFP was also observed in the other chaperone mutant *sdf2-2* (Fig. S3), suggesting that the SDF2-ERdj3-BiP complex is involved in maintaining the protein abundance of ERECTA.

Kifunensine (Kif) is an inhibitor of ER α-mannosidase, which prevents protein degradation via the ERAD pathway (Hüttner et al., 2014; Chen et al., 2020). The expression of ERECTA-YFP (*er-105* complementary) was significantly enhanced by Kif or MG-132 treatment (Fig. 2G-I). However, these effects were completely abolished in the *erdj3b-1* mutant (Fig. 2J-L), as supported by the quantitative analysis of ERECTA-YFP fluorescence intensities in stomatal lineage cells (Fig. 2M). Collectively, our results indicated that the SDF2-ERdj3B-BiP complex was involved in the modulation of ERECTA protein abundance.

To test the possible influence of the *erdj3b-1* mutation on intracellular trafficking of ERECTA-YFP, we used brefeldin A (BFA), an inhibitor of ADP-ribosylation factor guanine-nucleotide exchange factors (Geldner et al., 2003; Langhans et al., 2011; Naramoto et al., 2014; Qi et al., 2020). Application of 50 µM BFA for 1 h resulted in aggregation of ERECTA-YFP in 'BFA-body' structures. After a 1 h water washout, the BFA bodies disappeared and ERECTA-YFP relocated to the PM (Fig. 2N-P; Fig. S4). Although the expression level of ERECTA-YFP in *erdj3b-1* was lower than that in the wild-type, the response of ERECTA-YFP to BFA treatment in *erdj3b-1* was similar to that in the wild-type (*er-105* complementary), indicating that the *erdj3b* mutation has no discernible consequence on the intracellular trafficking of ERECTA (Fig. 2Q-S).

The chaperone complex is required for the subcellular dynamics of ERL1 and ERL2

ERL1:ERL1-YFP (*erl1-5* complementary) plants displayed a predominant localization of ERL1-YFP at the PM (Fig. 3A). In the *erdj3b-1* mutant background, ERL1-YFP exhibited a ring-like structure surrounding the nucleus (Fig. 3B). The results of quantitative image analysis demonstrated that in the *erl1-5* stomatal precursor cells, ERL1-YFP displayed partial colocalization with an ER marker mCherry-HDEL (Fig. 3C,G). However, in *erdj3b-1* precursor cells, ERL1-YFP highly colocalized with mCherry-HDEL in close proximity to the nucleus (Fig. 3D,G). Meanwhile, the fluorescence level of ERL1-YFP was decreased at the PM, which was labeled by FM4-64 (Fig. 3E-G). The ER retention of ERL1-YFP in *erdj3b-1* was recapitulated in the *sdf2-2* mutant (Fig. S5A,B), suggesting that the functional SDF2-ERdj3B-BiP chaperone complex is required for the transport of the ERL1 protein from the ER to the PM.

To further check the effects of *erdj3b-1* mutation on ERL1 retention in the ER, we performed the Endo-H assay using the ERL1-FLAG proteins extracted from *erdj3b-1* plants. In contrast to the two bands with similar intensity that were observed in wild-type *ERL1-FLAG* plants, the *erdj3b-1* mutant produced a stronger lower band of ERL1-FLAG (cleaved protein) after Endo-H digestion, demonstrating that the *erdj3b-1* mutation induced an increase in the amount of ERL1-FLAG that remained in the ER (Fig. 3H). By contrast, the ERECTA-FLAG proteins extracted from wild-type and *erdj3b-1* plants showed a similar sensitivity to Endo-H digestion (Fig. S5C), indicating the distinct effects of the *erdj3b-1* mutation on ERL1 and ERECTA.

We also monitored the BFA responses of ERL1-YFP in the *erdj3b-1* mutant. In the epidermis of *erl1-5* precursor cells, ERL1-YFP was sensitive to 50 µM BFA treatment by forming BFA bodies (Fig. 3I,J). However, ERL1-YFP in *erdj3b-1* mutant failed to colocalized with FM4-64 in the BFA bodies (Fig. 3K,L). Treatment with wortmannin (Wm), which can cause a fusion of multivesicular bodies/late endosomes by inhibiting phosphatidylinositol-3 and phosphatidylinositol-4 kinases (Foissner et al., 2016; Qi et al., 2020), was found to induce the dilation of late endosomal ERL1-YFP signals (Fig. 3M,N). However, the formation of these dilated ERL1-YFP-positive 'Wm bodies' was suppressed in *erdj3b-1* (Fig. 3O,P). These results suggested that the defective transport of ERL1 to PM via the secretion pathway in *erdj3b-1* might lead to a reduction of PM localization and consequent internalization of ERL1.

ERL2-YFP in the *erdj3b-1* mutant, like ERL1-YFP, lost its predominant localization at the PM and accumulated mostly in the ER (Fig. S5D,E). Consistently, ERL2-FLAG proteins extracted from *erdj3b-1* plants displayed hypersensitivity to Endo-H treatment (Fig. S5F). Therefore, the ER-resident chaperone complex SDF2-ERdj3B-BiP modulates ERECTAf receptors in distinct manners, i.e. by affecting the protein abundance for ERECTA versus the subcellular dynamics for ERL1 and ERL2.

BRI1, TMM, and the auxin transporters AUX1 and PIN3 are also involved in stomatal development (Nadeau and Sack, 2002; Swarup et al., 2004; Kim et al., 2012; Le et al., 2014). However, none of them exhibited visible changes in localization in the *erdj3b-1* stomatal lineage cells (Fig. S6). Thus, the impact of SDF2-ERdj3B-BiP on ERECTAf receptors does not seem to be a universal phenomenon.

Genetic relationship of the chaperone complex with ERECTAf receptors in regulating stomatal development

Compared with wild type, no obvious stomatal phenotypes were observed in the *erdj3b-1* mutant leaf epidermis (Fig. 4A,B). As reported previously (Shpak et al., 2005), *er-105* produced an excessive number of arrested stomatal lineage cells that were unable to differentiate into mature stomata (Fig. 4C,K, colored in pink).

Development (2022) 149, dev200892. doi:10.1242/dev.200892

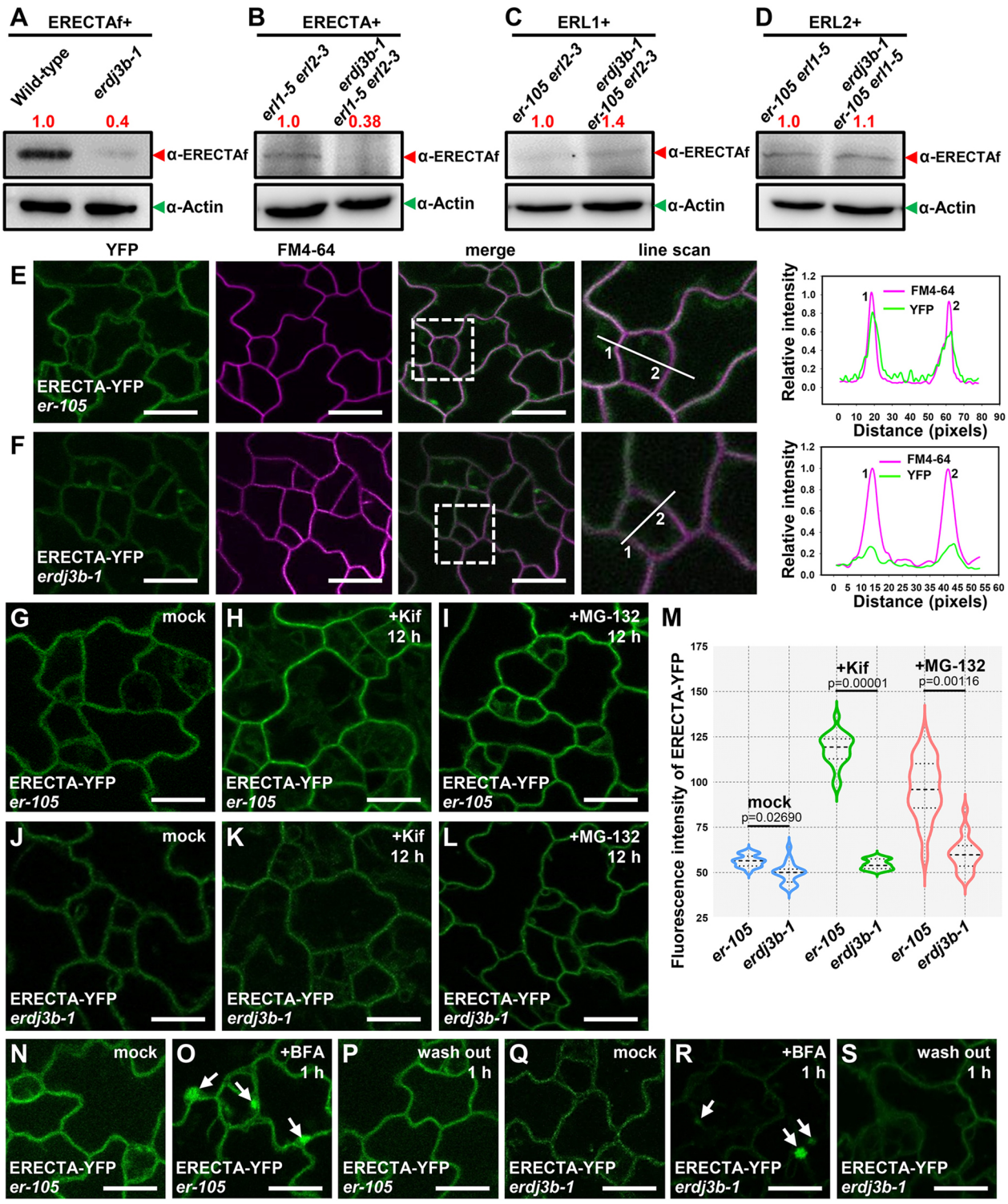

Fig. 2. Mutation of *erdj3b* affects the protein abundance but not the localization of ERECTA. (A-D) Immunoblotting analysis of protein amount using antibodies that recognize all ERECTAf proteins (red arrowhead). The numbers above the upper panel are relative ratios of mean gray values of bands to those of wild type samples. The lower panel shows the loading control detected with anti-actin (green arrowhead). (E) Colocalization analysis of ERECTA-YFP (*er-105* complementary) (green) and FM4-64 dye (magenta). (F) In *erdj3b-1*, ERECTA-YFP fluorescence intensity was greatly reduced at the PM, compared with that of FM4-64. Images in the fourth panels are magnified views of dotted white boxes in the third panels. ERECTA-YFP and FM4-64 fluorescence intensity profiles were quantified (rightmost panel) along a transect crossing stomatal precursor cells (line scan, indicated by a white line). (G-L) The protein level of ERECTA-YFP was enhanced after a 12 h treatment with 20 µM kifunensine (Kif) or 40 µM MG-132, but not after treatment in the *erdj3b-1* mutant background. (M) Quantification of fluorescence intensity in stomatal precursor cells. Kif- and MG-132-induced increase in ERECTA-YFP levels was significantly suppressed in the *erdj3b*-1 mutant. Two-tailed unpaired Student's *t*-test was performed between *er-105* and *erdj3b-1* (n=21). Dotted lines indicate the 25th-75th percentiles and dashed lines indicate the median. (N-S) Application of 50 µM BFA induced aggregation of ERECTA-YFP in BFA bodies (white arrows), an effect that was reversed after washout. ERECTA-YFP in *erdj3b-1* displayed a similar response to BFA. Images are representative of three independent experiments. Scale bars: 20 µm.

Development (2022) 149, dev200892. doi:10.1242/dev.200892

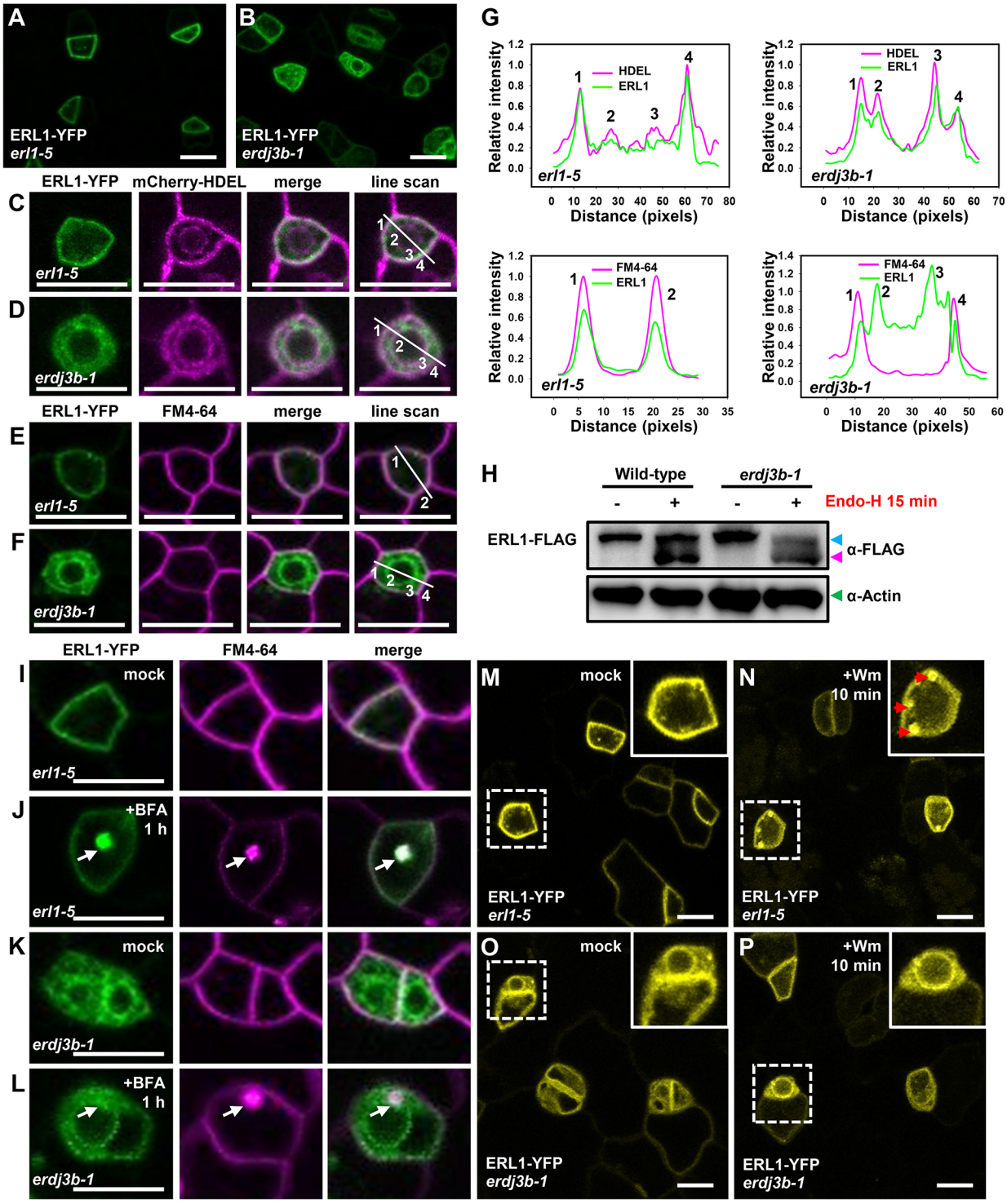

Fig. 3. Mutation of *erdj3b* mainly affects the subcellular localization of ERL1. (A,B) ERL1-YFP (*erl1-5* complementary) predominantly localized at the PM of stomatal lineage cells. In the *erdj3b-1* mutant, ERL1-YFP was found in a ring-like structure surrounding the nucleus. (C-G) Colocalization of ERL1-YFP with the ER marker mCherry-HDEL (C,D) in *erdj3b-1* stomatal precursor cells was confirmed by quantitative analysis of fluorescence intensity profiles (G, top panels). Colocalization of ERL1-YFP with the FM4-64 dye at the PM (E,F) was reduced in *erdj3b-1*. Line scan profiles (G, lower panels) demonstrate the change of ERL1-YFP localization from the PM to the ER. (H) Immunoblotting analysis of ERL1-FLAG in the Endo-H assay. ERL1-FLAG extracted from *erdj3b-1* plants was sensitive to Endo-H, showing a stronger lower band (cleaved proteins, pink arrowhead). (I-L) After 1 h treatment with 50 µM BFA, ERL1-YFP colocalized with FM4-64 in BFA bodies (white arrow). However, ERL1-YFP in the *erdj3b-1* mutant failed to colocalize with FM4-64 in BFA bodies. (M-P) Application of 25 µM wortmannin (Wm, 10 min) induced the formation YFP-positive Wm bodies (red arrows in inset) but not in *erdj3b-1* mutant precursor cells. Images are representative of three independent experiments. Scale bars: 20 µm.

Development (2022) 149, dev200892. doi:10.1242/dev.200892

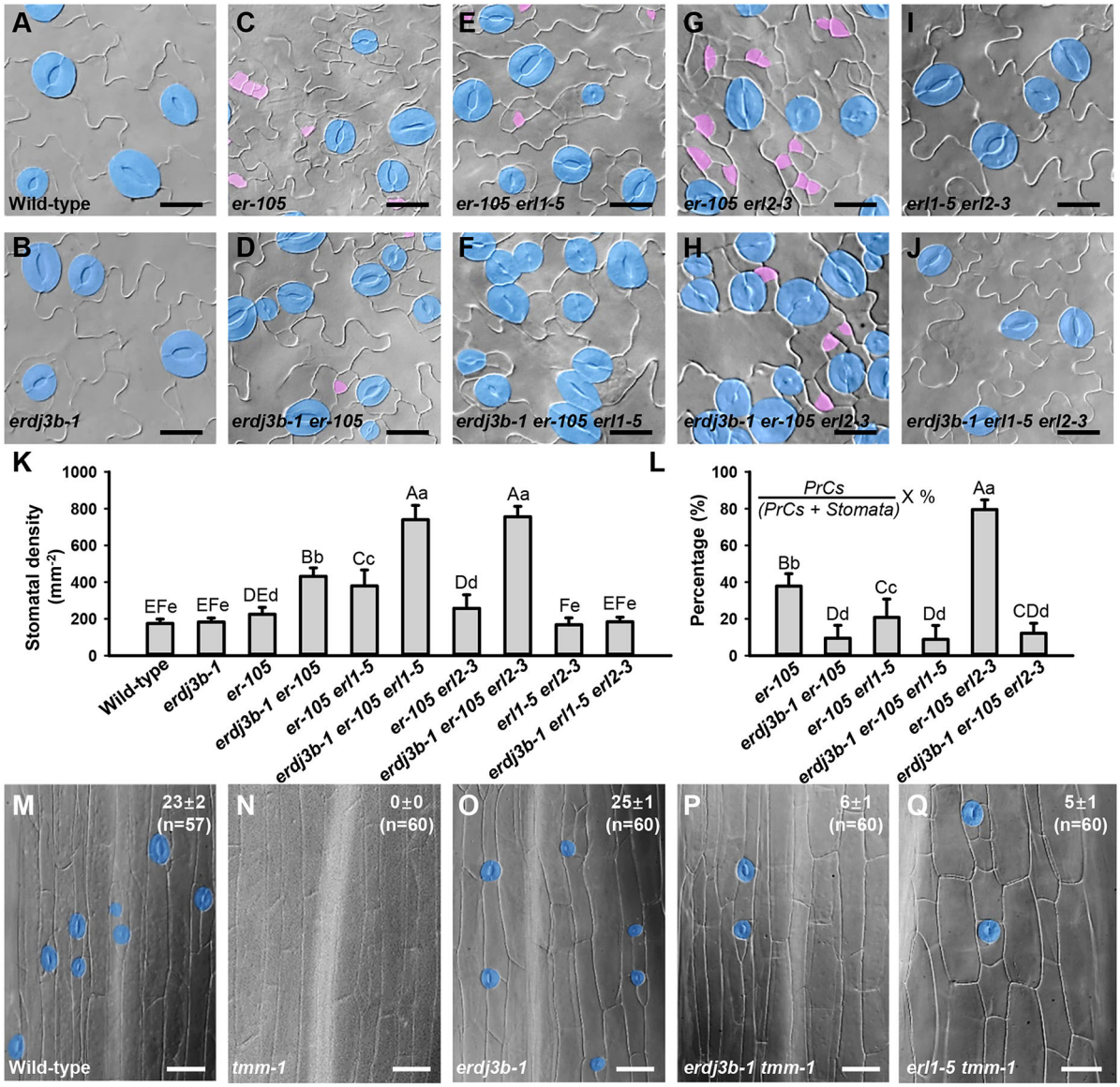

Fig. 4. ERECTAf receptors are distinctly regulated by the ERQC system. (A-J) DIC images of 12-day-old cotyledons. Mature stomata and PrCs are highlighted in blue and pink, respectively. Mutation of *erdj3b* promoted the differentiation of PrCs into mature stomata and stomatal clusters in the *er-105*, *er-105 erl1-5* and *er-105 erl2-3* lines. (K,L) Quantitative analysis of stomatal density and percentage of PrCs over the total number of PrCs and stomata. Values are mean±s.d. (*n*=18). Data were analyzed using one-way ANOVA with Tukey's post hoc test. The different uppercase and lowercase letters indicate significant differences at 1% and 5%, respectively. (M-Q) Mutation of *erdj3b*, like *erl1*, could restore the stomatal formation of hypocotyls in the *tmm-1* mutant. The numbers in the upper right corners indicate the number of stomata per hypocotyl (mean±s.d.). Scale bars: 20 µm.

However, the additional *erdj3b* mutation in *er-105* plants reduced the percentage of small PrCs (over the total number of PrCs and mature stomata) and induced stomatal clusters, leading to an increased stomatal density (Fig. 4D,K). Similar phenotypes were also found in the *sdf2-2 er-105* mutant, confirming the requirement of a functional SDF2-ERdj3B-BiP complex in stomatal development (Fig. S7A-F). Introduction of *ERDJ3B-GFP* restored the appearance of small PrCs in the *erdj3b-1 er-105* epidermis (Fig. S7G,H). ERDJ3B-GFP highly colocalized with the ER marker mCherry-HDEL, supporting that ERdj3B, as predicted, is an ER-resident molecular chaperone (Fig. S7I,J).

Mutation of *erl1* was able to resume the stomatal precursor cell differentiation in *er-105* (Fig. 4E) (Shpak et al., 2005). However, comparing with the *er-105 erl1-5* double mutant, the *erdj3b-1 er-105 erl1-5* triple mutant exhibited a more severe stomatal clustering phenotype and increased the number of mature stomata (Fig. 4F,K), indicating that the *erdj3b* mutation caused the dysfunction of other regulator(s), like ERL2, apart from ERECTA and ERL1.

In contrast to the function of the *erl1* mutation, an additional *erl2* mutation enhanced the formation of excessive PrCs in the *er-105* mutant (Fig. 4G,L). The *erdj3b-1 er-105 erl2-3* triple mutant displayed a reduced percentage of PrCs compared with the *er-105 erl2-3* double mutant (Fig. 4H,L). We suspected that the action of ERdj3B is possibly through ERL2, which is antagonistic to ERL1 in repressing precursor cell differentiation. However, the *erl1-5 erl2-3* mutant displayed normal stomatal development (Fig. 4I). No observable change of stomatal phenotype was found in the *erdj3b-1 erl1-5 erl2-3* mutant (Fig. 4J), suggesting the redundant function of ERECTA in stomatal development control, although the abundance of ERECTA receptors was reduced owing to the *erdj3b-1* mutation.

Development (2022) 149, dev200892. doi:10.1242/dev.200892

Furthermore, we checked the impact of the *erdj3b-1* mutation on stomatal development in the hypocotyl, where TMM acts to dampen ERECTAf-mediated signaling (Shpak et al., 2005). In agreement with the statement that ERdj3B functions in stomatal differentiation, mutation of *erdj3b-1* conferred stomatal production in *tmm-1* hypocotyls, mimicking the stomatal phenotype in *tmm-1 erl1-5* mutant hypocotyls (Fig. 4M-Q).

The YODA (YDA)-mitogen-activated protein kinase (MAPK) cascade acts downstream of the TMM-ERECTAf receptor complexes in stomatal development (Lampard et al., 2008, 2014). Notably, the *erdj3b-1* mutation neither affected the excessive stomatal phenotype of the loss-of-function *yoda* mutant, nor altered the stomata-less phenotypes of the constitutively active *CA-YDA* plants (Fig. 5A-D,M), indicating that *ERDJ3B* genetically functions upstream of the YODA-MAPK cascade. Loss of BASL function in the *basl-2* allele has been shown to induce the formation of clustered PrCs in the epidermis (Dong et al., 2009; Zhang et al., 2015) (Fig. 5E). However, the *erdj3b-1* mutation failed to convert these small PrCs into mature stomata, indicating that ERdj3B is unlikely to act in the same pathway with BASL (Fig. 5F,M,N). On the contrary, the stomatal phenotypes induced by overexpression of *EPF1*, *EPF2* or *EPFL9* were abolished or reduced in the *erdj3b-1* mutant background (Fig. 5G-N), further confirming a role for ERdj3B in ERECTAf receptor-mediated signaling during stomatal development.

DISCUSSION

The functions of secretory EPF/EPFL peptides and TMM-ERECTAf receptors in *Arabidopsis* stomatal development have been intensively investigated (Yang and Sack, 1995; Shpak et al., 2005; Hara et al., 2007; Hunt and Gray, 2009; Dong and Bergmann, 2010; Pillitteri and Torii, 2012; Qu et al., 2017). Three ERECTAf receptors redundantly govern the initial decision of stomatal lineage and distribution pattern in the epidermis, but individual members contribute differently to stomatal lineage cell differentiation. A question that arises is what determines the distinct roles of ERECTAf receptors that have high homology.

In eukaryotic cells, the majority of membrane receptor proteins are processed in the ER and controlled by the ERQC system. Only correctly folded receptors can exit from the ER and be transported to their final PM destination via the secretory pathway. Improperly or incompletely folded proteins are retained in the ER for further folding or ultimately degraded by ERAD (Fig. 6). Several conserved N-glycosylation motifs like N(X)S/T have been predicted in the ectodomain (LRR) of the ERECTAf receptors (Chakraborty et al., 2019). Here, we experimentally confirmed that inhibition of protein N-glycosylation by TM significantly affects the protein abundance and subcellular distribution of all three ERECTAf receptors. Whether the N-glycosylation differences cause the functional diversity of ERECTAf receptors needs to be further investigated. However, we found that the dysfunction of the

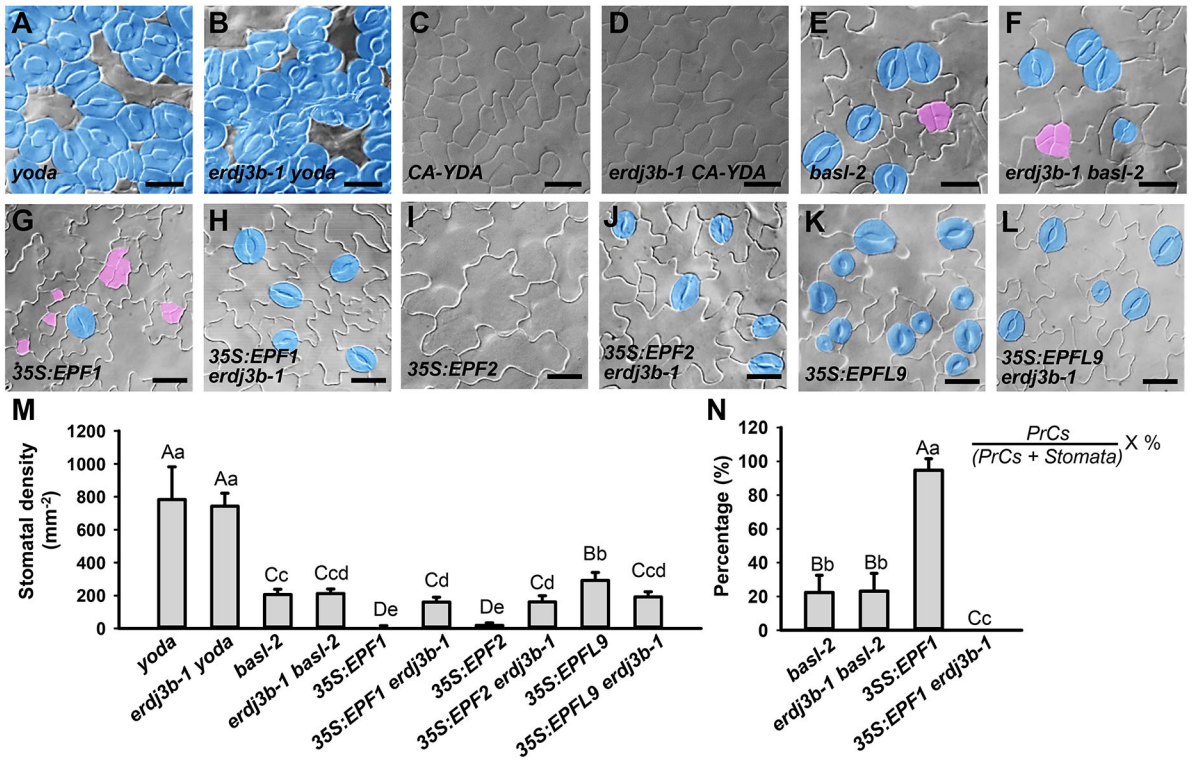

Fig. 5. Function of ERdj3B is required for signaling transduction of peptide ligands upstream of YODA. (A,B) Mutation of *erdj3b* had no impact on the stomatal phenotype in *yoda*. Large stomatal clusters were found in both *yoda* (A) and in *erdj3b-1 yoda* (B) mutants. (C,D) No stoma was found in the *CA-YDA* (C) and *erdj3b-1 CA-YDA* (D). (E,F) Mutation of *erdj3b* had no impact on the stomatal phenotype of *basl-2*. Similar stomatal clusters and small-cell clusters (highlighted in pink) were found in both *basl-2* (E) and *erdj3b-1 basl-2* (F) mutants. (G,H) Overexpression of *EPF1* promoted over-proliferative divisions in epidermal cells (highlighted in pink) (G), but the effect of *EPF1* overexpression was abolished in a *35S:EPF1 erdj3b-1* transgenic line (H). (I,J) Overexpressing *EPF2* inhibited stomatal production in a *35S:EPF2* transgenic (I), but stomatal production was resumed in the *35S:EPF2 erdj3b-1* transgenic (J). (K,L) Overexpression of *EPFL9* promoted stomatal production in a *35S:EPFL9* transgenic line (K), and the stomatal production was normal in a *35S:EPFL9 erdj3b-1* transgenic line (L). (M,N) Quantitative analysis of stomatal density (M) and percentage of PrCs (N) over the total number of PrCs and stomata. Values are mean±s.d. (n=18). Data were analyzed using one-way ANOVA with Tukey's post hoc test. The different uppercase and lowercase letters indicate significant differences at 1% and 5%, respectively. Scale bars: 20 µm.

Development (2022) 149, dev200892. doi:10.1242/dev.200892

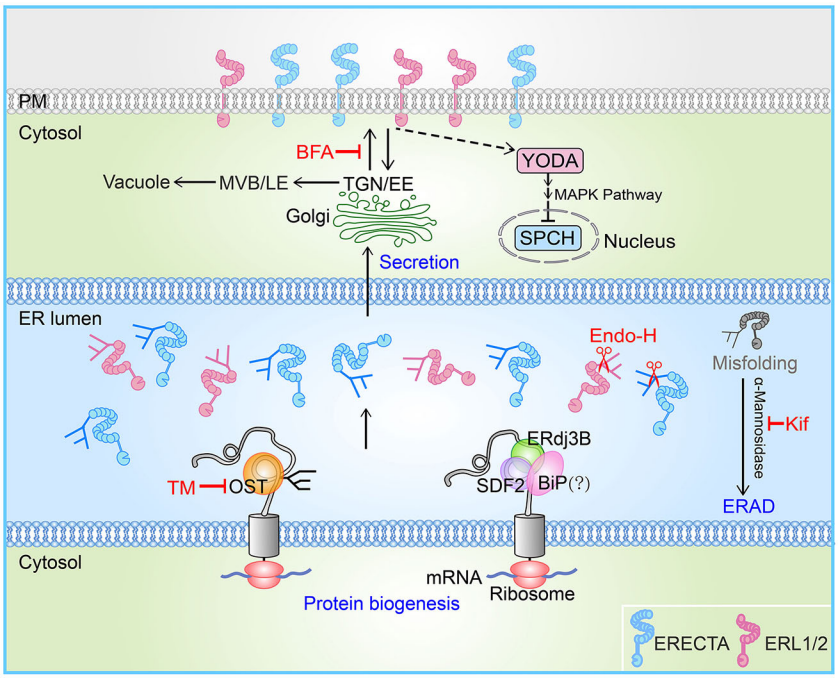

Fig. 6. Model of the SDF2-ERdj3B-BiP chaperone complex regulating stomatal development. Schematic model of regulation of ERECTAf receptors by ERQC. Inhibition of N-glycosylation by TM significantly affects the protein abundance and subcellular localization of ERECTAf receptors. Endo-H primarily cleaves N-linked glycans of ER-localized proteins. The function of the SDF2-ERdj3B-BiP chaperone complex is required for ERECTAf protein biogenesis in the ER lumen and transport of ERECTAf proteins from the ER to the plasma membrane (PM), where they finally activate the downstream YODA-MAPK cascade to regulate stomatal development. Improperly or incompletely folded proteins are retained in the ER for further folding or ultimately degraded by ERAD. Kifunensine, an inhibitor of ER mannosidase, prevents the degradation of misfolded protein via the ERAD pathway. Multivesicular bodies/late endosomes, MVB/LE; oligosaccharyltransferase, OST; SPEECHLESS transcription factor, SPCH; trans-Golgi network/early endosome, TGN/EE.

ER-resident chaperone complex SDF2-ERdj3B-BiP differentially affects the biogenesis and subcellular dynamics of ERECTAf receptors.

ERECTA is broadly expressed in the epidermis and plays a predominant role overlapping with ERL1 and ERL2 in stomatal patterning control. In contrast to the normal stomatal phenotypes of *erl1*, *erl2* and *erl1 erl2*, the single mutation of *erecta* confers an increase of stomatal lineage cells. Although the abundance of ERECTA is reduced in the *erdj3b* mutant, the intracellular trafficking of the remaining ERECTA protein is normal. The additional mutation of *erdj3b* has no impact on the *erl1 erl2* stomatal phenotype due to the presence of functional ERECTA. This functional insensitivity of ERECTA, unlike ERL1 and ERL2, to dysfunction of the chaperone complex maintains a minimum signaling that enforces the stomatal 'one-cell-spacing' rule.

We found that the transcriptional level of *ERECTA* was not altered by the *erdj3b* mutation. The effects of Kif and MG-132 treatment on the abundance of ERECTA in the *erdj3b-1* mutant were limited, suggesting that the reduction of ERECTA proteins was mainly caused by the downregulation of protein synthesis, but not of protein degradation (Fig. 6). Similarly, the protein levels of EFR, another LRR receptor kinase, in total extracts were found to be strongly reduced in the *sdf2-2* background, although the transcription of *EFR* was not changed (Nekrasov et al., 2009). Accumulation of misfolded proteins in the ER triggers the unfolded protein response. In yeast and mammalian cells, the unfolded protein response leads to a halt of protein synthesis through the action of protein kinase RNA-like ER kinases (PERKs) (Hetz, 2012). The release of BiP from PERK results in PERK autophosphorylation and subsequently inhibits protein translation via the phosphorylation of eIF2α, the key translation initiation factor. *Arabidopsis* has eIF2α but no PERK homolog has been found (Kanodia et al., 2020). In response to dithiothreitol (DTT)-induced ER stress, GENERAL CONTROL NON-DEREPRESSIBLE 1 (GCN1) and GCN2 promote the phosphorylation of eIF2α (Izquierdo et al., 2018). In maize, ER-stress induces the decline of protein translation efficiency because of the sequestration of mRNAs in stress granules (Kanodia et al., 2020). Therefore, in response to ER stress, like yeast and mammalian cells, plants have ways to relieve the protein overload in the ER by downregulating protein synthesis.

Both ERL1 and ERL2 are specifically expressed in stomatal lineage cells and exhibit hypersensitivity to ER stress. It was demonstrated that EPF1-induced ERL1 internalization and trafficking, for which TMM is essential, are required for the function of ERL1 in restricting stomatal lineage cell differentiation. However, EPFL9 competes with EPF1 by trigging the retention of ERL1 in the ER (Qi et al., 2020). In agreement with this, the arrested stomatal differentiation in *erecta* leaves and *tmm* hypocotyls is rescued in an *erdj3b-1* mutant background. In addition, the effects of *EPF1* and *EPFL9* overexpression on stomatal phenotypes are abolished in the *erdj3b-1* mutant, further supporting the finding that ER-resident molecular chaperones are required for the subcellular dynamics and function of ERL1.

ERL2, like TMM, can heteromerize with ERECTA and ERL1 to modulate signaling (Ho et al., 2016). Here, we provide evidence that ERL2 localization and function are modulated by SDF2-ERdj3B-BiP. An additional *erdj3b* mutation in *erecta erl1* plants produced excessive stomata in clusters, resembling the phenotypes of the *erecta erl1 erl2* triple mutant. Mutation of *erdj3b* caused the majority of the ERL1 protein to be retained in the ER and failed to transport to the PM, consequently alleviated the repressive effect of ERL1 on stomata lineage cell differentiation in *erecta erl2* double mutants. The study of the molecular chaperone complex SDF2-ERdj3B-BiP as a modulator of ERECTAf receptors in the ER will be helpful to further reveal the finely tuned mechanism of stomatal patterning and development.

MATERIALS AND METHODS

Plant materials and growth conditions

Arabidopsis accession Columbia (Col-0) was used as wild-type. The *erdj3b-1* (SALK_113364), *erl1-5* (SALK_019567), *erl2-3* (GK_486E03) and *sdf2-2* (SALK_141321) were ordered from the *Arabidopsis* Biological Resource Center (https://abrc.osu.edu). The following higher-order mutants and marker lines were generated by crossing: *erdj3b-1 er-105*, *er-105 erl2-*

Development (2022) 149, dev200892. doi:10.1242/dev.200892

3, *erdj3b-1 er-105 erl2-3*, *er-105 erl1-5*, *erdj3b-1 er-105 erl1-5*, *erl1-5 erl2-3*, *erdj3b-1 erl1-5 erl2-3*, *erdj3b-1 tmm-1*, *sdf2-2 er-105*, *erdj3b-1 yoda*, *erdj3b-1 CA-YDA*, *erdj3b-1 basl-2*, *ERECTA:ERECTA-YFP erdj3b-1*, *ERECTA:ERECTA-YFP sdf2-2*, *ERL1:ERL1-YFP erdj3b-1*, *ERL1:ERL1-YFP 35S:mCherry-HDEL*, *ERL1:ERL1-YFP 35S:mCherry-HDEL erdj3b-1*, *ERL1:ERL1-YFP sdf2-2*, *ERL2:ERL2-YFP erdj3b-1*, *ERDJ3B:ERDJ3B-GFP 35S:mCherry-HDEL*, *PIN3:PIN3-GFP erdj3b-1*, *AUX1:AUX1-YFP erdj3b-1*, *BRI1:BRI1-GFP erdj3b-1*, *SUPER:ERECTA-FLAG erdj3b-1*, *SUPER:ERL1-FLAG erdj3b-1*, *SUPER:ERL2-FLAG erdj3b-1* and *ERDJ3B:ERDJ3B-GFP 35S:mCherry-HDEL*. Sterilized seeds were grown on half strength of Murashige and Skoog (1/2 MS) medium supplemented with 1% sucrose and 0.8% agar at 22°C in a growth room with a 16 h light/8 h dark light regime.

Plasmid construction and plant transformation

To obtain *ERDJ3B:ERDJ3B-GFP*, the full-length genomic DNA of *ERDJ3B* without T-Nos driven by its native promoter was cloned into the pCAMBIA1300-GFP vector (Cambia). For *SUPER:ERECTA-FLAG*, *SUPER:ERL1-FLAG* and *SUPER:ERL2-FLAG*, the full-length genomic DNA of *ERECTA*, *ERL1* and *ERL2* without T-Nos was cloned into the pCAMBIA1300-FLAG vector. For the *ERECTA:ERECTA-YFP*, *ERL1:ERL1-YFP*, *ERL2:ERL2-YFP* and *SERK3:SERK3-YFP* constructs, the genomic coding regions of *ERECTA*, *ERL1*, *ERL2* and *SERK3* (from ATG to immediately ahead of the stop codon) were amplified and cloned into pENTR/D-TOPO (Invitrogen). Next, the promoter regions were amplified and inserted into the NotI site of pENTR/D-TOPO vectors carrying the respective genomic regions. Then, the entry clone was recombined by the Clonase II enzyme mix (Invitrogen) into the destination vector pHGY (Kubo et al., 2005) for expression in plants. To obtain the *35S:EPF1*, *35S:EPF2* and *35S:EPFL9* constructs, the cDNA of *EPF1*, *EPF2* and *EPFL9* was obtained by PCR amplification. Then the fragments were cloned into a pCAMBIA1300 vector under control of the 35S promoter. Primers used for plasmid constructs are listed in Table S1. All constructs were transformed into the *Agrobacterium tumefaciens* strain EHA105, and then transformed into wild-type or *erdj3b-1* mutant seedlings by floral dipping. Transgenic plants were selected on 1/2 MS medium containing 25 µg/ml hygromycin.

Real-time quantitative PCR

Total RNA from 5-day-old wild-type and *erdj3b-1* seedlings was extracted using HiPure Plant RNA Mini Kit (Magen Biotechnology). Reverse transcription was performed using PrimeScript RT Reagent Kit (TaKaRa). Amplified *ACTIN2* gene was used as an internal control. Real-time quantitative PCR experiments were repeated independently for three times. The data were averaged, and cDNA was amplified using Hieff qPCR SYBR Green Master Mix (Yeasen Biotechnology) with Roche Applied Science Light Cycler 96. Primers specific to target genes used for real-time quantitative PCR are listed in Table S1.

Immunoblotting analysis

For endogenous ERECTAf protein analysis, the peptide containing amino acids 25-332 of the ERECTA protein sequence was used to produce an ERECTA family-specific rabbit polyclonal antibody (Abmart, Shanghai, China). Total proteins were extracted from etiolated 4-day-old seedlings of the Col-0, *erdj3b-1*, *er-105 erl1-5*, *erdj3b-1 er-105 erl1-5*, *er-105 erl2-3*, *erdj3b-1 er-105 erl2-3*, *erl1-5 erl2-3* and *erdj3b-1 erl1-5 erl2-3* using protein extraction buffer [100 mM Tris-HCl, pH 7.5, 150 mM NaCl, 2 mM EDTA, 2% Triton X-100, 20% glycerol, 20 mM NaF, 1 mM phenylmethanesulfonyl fluoride, 1× protease inhibitor cocktail (Roche)]. The homogenate was centrifuged at 5000 ***g*** for 30 min to remove debris. Supernatants were then used for immunoblotting analysis using the anti-ERECTAf antibody (1:5000). Actin was used as the loading control and detected by an anti-actin antibody (1:5000, CWBIO, CW0264M).

For TM, CHX or MG-132 treatment, *SUPER:ERECTA-FLAG*, *SUPER:ERL1-FLAG* and *SUPER:ERL2-FLAG* seedlings were first grown on 1/2 MS medium plates for 2 days, and then treated with 60 ng/mL TM or in combination with 100 µM CHX or 40 µM MG132 for 48 h. The total proteins were extracted as described above. Supernatants were used for immunoblotting analysis. Anti-FLAG (1:10,000, Sigma-Aldrich, F1804-50UG) and anti-actin (1:5000) antibodies were used for immunoblotting analysis.

Endo-H enzymatic assay

Total proteins were extracted from 4-day-old seedlings of *SUPER:ERECTA-FLAG*, *SUPER:ERECTA-FLAG erdj3b-1*, *SUPER:ERL1-FLAG*, *SUPER:ERL1-FLAG erdj3b-1*, *SUPER:ERL2-FLAG* and *SUPER:ERL2-FLAG erdj3b-1*. For TM treatment, *SUPER:ERECTA-FLAG*, *SUPER:ERL1-FLAG* and *SUPER:ERL2-FLAG* seedlings were first grown on 1/2 MS medium plates for 2 days, and then treated with 0.01% DMSO or 60 ng/ml TM for 48 h. Extracted proteins were digested with Endo-H (New England Biolabs) for 5-60 min at 37°C before immunoblotting analysis. Anti-FLAG (1:10,000) and anti-actin (1:5000) antibodies were used for immunoblotting analysis.

Microscopy and image analysis

To obtain differential interference contrast (DIC) images, cotyledons or hypocotyls were cleared with a destaining solution (containing 75% ethanol and 25% acetic acid) overnight at room temperature. After treatment with a basic solution (7% NaOH in 60% ethanol) for 15 min at room temperature, the samples were rehydrated via an ethanol series (40%, 20% and 10%) for 20 min at each step. Images were captured using an Olympus BX51 microscope.

For FM4-64 (Invitrogen) staining, cotyledons of 4-day-old seedlings of the *ERECTA:ERECTA-YFP*, *ERECTA:ERECTA-YFP erdj3b-1*, *ERL1:ERL1-YFP* and *ERL1:ERL1-YFP erdj3b-1* lines were immersed into 2 µM FM4-64 for 30 min. For propidium iodide staining, cotyledons of 4-day-old seedlings were stained with 0.1% propidium iodide for 1 min. Confocal images were captured using an Olympus FV1000-MPE laser scanning confocal microscope. The excitation/emission spectra are 488 nm/501-528 nm for GFP/YFP and 543 nm/600-620 nm for mCherry, FM4-64 and propidium iodide. The line scan across the stomatal precursor cells were analyzed with the Plot Profile function of ImageJ (https://imagej.nih.gov/ij/).

Pharmacological treatment

To assess the impact of TM on stomatal development, 10-day-old seedlings grown in 1/2 MS medium supplemented with 30, 60, 120 and 240 ng/ml TM (Macklin) were used. Two-day-old *ERECTA:ERECTA-YFP er-105*, *ERL1:ERL1-YFP erl1-5*, *ERL2:ERL2-YFP*, *SERK3:SERK3-YFP* and *BRI1:BRI1-GFP* seedlings were treated with 60 ng/ml TM for 24 or 48 h before imaging.

For kifunensine or MG-132 treatment, 3-day-old seedlings of *ERECTA:ERECTA-YFP* and *ERECTA:ERECTA-YFP erdj3b-1* were treated with 20 µM kifunensine (MedChemExpress) or 40 µM MG-132 (Merck) for 12 h. For BFA treatment, 4-day-old seedlings were first immersed into 2 µM FM4-64 for 30 min before treatment with 50 µM BFA solution (Macklin) for 60 min. For BFA washout, seedlings were rinsed in water for 60 min. For wortmannin treatment, *ERL1:ERL1-YFP erl1-5* and *ERL1:ERL1-YFP erdj3b-1* seedlings were treated with 25 µM wortmannin (Selleck) for 10 min before imaging.

Quantification and statistical analysis

For quantitative analysis of relative protein abundance of ERECTAf receptors, the mean gray value of bands recognized by anti-ERECTAf antibodies in immunoblots were measured using ImageJ. The relative ratios of mean gray value of bands were used in the pairwise comparison of protein abundance. Data shown represent one of three independent experiments.

For quantitative analysis of the effects of kifunensine or MG-132 on ERECTA-YFP expression, the mean intensity values of YFP fluorescence from stomatal precursor cells were measured using ImageJ. Data shown are from one experiment representative of three independent experiments.

For quantitative analysis of *Arabidopsis* stomatal phenotypes, the numbers of mature stomata and PrCs in a region of 0.2 mm^2 from the same quadrant of 12 adaxial cotyledons were scored. Small epidermal cells with an area equal to or smaller than a normal stomatal GMC were classified

as PrCs (Le et al., 2014). PrC percentage is indicated as the number of PrCs over the total number of PrCs and mature stomata.

All statistical analyses were conducted with SPSS 25.0 software. To compare two normally distributed groups, *F*-tests were performed first, and then unpaired two-tailed *t*-tests were used. For multiple comparisons between normally distributed groups, one-way ANOVA followed by Tukey's post hoc test was used.

Acknowledgements
We thank Prof. Zu-Hua He (CAS Center for Excellence in Molecular Plant Sciences, Chinese Academy of Sciences, Shanghai, China) for the gifts of *er-105* mutant seeds and Prof. Wei-Cai Yang (Institute of Genetics and Developmental Biology, Chinese Academy of Sciences, Beijing, China) for the gift of mCherry-HDEL plasmid. We thank Wei Wang (Swedish University of Agricultural Sciences, Sweden) for critical reading of the manuscript and English editing. We thank Jing-Quan Li (Plant Science Facility of the Institute of Botany, Chinese Academy of Sciences) for her excellent technical assistance of confocal microscopy analysis.

Competing interests
The authors declare no competing or financial interests.

Author contributions
Software: C.-R.Z., H.-C.L.; Validation: K.-Z.Y., C.-R.Z., X.-Y.X.; Formal analysis: K.-Z.Y., C.-R.Z., J.-L.Y., Z.-B.F.; Investigation: Y.-J.L.; Resources: Y.-J.L., L.-Q.C., J.L.; Data curation: K.-Z.Y., C.-R.Z., Y.-J.L., J.-L.Y., H.-C.L., Z.-B.F., X.-Y.X.; Writing - original draft: K.-Z.Y., J.D., L.-Q.C., J.L.; Writing - review & editing: K.-Z.Y., C.-R.Z., J.D., L.-Q.C., J.L.; Visualization: C.-R.Z.; Supervision: J.D., L.-Q.C., J.L.; Project administration: K.-Z.Y., Y.-J.L., L.-Q.C.; Funding acquisition: K.-Z.Y., L.-Q.C., J.L.

Funding
This work was supported by grants from the National Natural Science Foundation of China (31871377 and 32070723 to K.-Z.Y.; 31970804 and 32170722 to J.L.; and 31470279 and 31872668 to L.-Q.C.).

References
Buchberger, A., Bukau, B. and Sommer, T. (2010). Protein quality control in the cytosol and the endoplasmic reticulum: brothers in arms. *Mol. Cell* **40**, 238-252. doi:10.1016/j.molcel.2010.10.001

Chakraborty, S., Nguyen, B., Wasti, S. D. and Xu, G. (2019). Plant Leucine-Rich Repeat Receptor Kinase (LRR-RK): structure, ligand perception, and activation mechanism. *Molecules* **24**, 3081. doi:10.3390/molecules24173081

Chen, T., Zhang, H., Niu, G., Zhang, S. and Hong, Z. (2020). Multiple N-glycans cooperate in balancing misfolded BRI1 secretion and ER retention. *Plant Mol. Biol.* **103**, 581-596. doi:10.1007/s11103-020-01012-z

Dong, J. and Bergmann, D. C. (2010). Stomatal patterning and development. *Curr. Top. Dev. Biol.* **91**, 267-297. doi:10.1016/s0070-2153(10)91009-0

Dong, J., MacAlister, C. A. and Bergmann, D. C. (2009). BASL controls asymmetric cell division in *Arabidopsis*. *Cell* **137**, 1320-1330. doi:10.1016/j.cell.2009.04.018

Foissner, I., Sommer, A., Hoeftberger, M., Hoepflinger, M. C. and Absolonova, M. (2016). Is Wortmannin-Induced reorganization of the trans-Golgi network the key to explain charasome formation? *Front. Plant Sci.* **7**, 756. doi:10.3389/fpls.2016.00756

Geldner, N., Anders, N., Wolters, H., Keicher, J., Kornberger, W., Muller, P., Delbarre, A., Ueda, T., Nakano, A. and Jürgens, G. (2003). The *Arabidopsis* GNOM ARF-GEF mediates endosomal recycling, auxin transport, and auxin-dependent plant growth. *Cell* **112**, 219-230. doi:10.1016/s0092-8674(03)00003-5

Hara, K., Kajita, R., Torii, K. U., Bergmann, D. C. and Kakimoto, T. (2007). The secretory peptide gene EPF1 enforces the stomatal one-cell-spacing rule. *Genes Dev.* **21**, 1720-1725. doi:10.1101/gad.1550707

Helenius, A. and Aebi, M. (2004). Roles of N-linked glycans in the endoplasmic reticulum. *Annu. Rev. Biochem.* **73**, 1019-1049. doi:10.1146/annurev.biochem.73.011303.073752

Hetz, C. (2012). The unfolded protein response: controlling cell fate decisions under ER stress and beyond. *Nat. Rev. Mol. Cell Biol.* **13**, 89-102. doi:10.1038/nrm3270

Ho, C.-M., Paciorek, T., Abrash, E. and Bergmann, D. C. (2016). Modulators of stomatal lineage signal transduction alter membrane contact sites and reveal specialization among ERECTA kinases. *Dev. Cell* **38**, 345-357. doi:10.1016/j.devcel.2016.07.016

Hong, Z., Kajiura, H., Su, W., Jin, H., Kimura, A., Fujiyama, K. and Li, J. (2012). Evolutionarily conserved glycan signal to degrade aberrant brassinosteroid receptors in *Arabidopsis*. *Proc. Natl. Acad. Sci. USA* **109**, 11437-11442. doi:10.1073/pnas.1119173109

Hunt, L. and Gray, J. E. (2009). The signaling peptide EPF2 controls asymmetric cell divisions during stomatal development. *Curr. Biol.* **19**, 864-869. doi:10.1016/j.cub.2009.03.069

Hüttner, S., Veit, C., Vavra, U., Schoberer, J., Dicker, M., Maresch, D., Altmann, F. and Strasser, R. (2014). A context-independent N-glycan signal targets the misfolded extracellular domain of *Arabidopsis* STRUBBELIG to endoplasmic-reticulum-associated degradation. *Biochem. J.* **464**, 401-411. doi:10.1042/BJ20141057

Izquierdo, Y., Kulasekaran, S., Benito, P., López, B., Marcos, R., Cascón, T., Hamberg, M. and Castresana, C. (2018). *Arabidopsis* nonresponding to oxylipins locus NOXY7 encodes a yeast GCN1 homolog that mediates noncanonical translation regulation and stress adaptation. *Plant Cell Environ.* **41**, 1438-1452. doi:10.1111/pce.13182

Jin, H., Yan, Z., Nam, K. H. and Li, J. (2007). Allele-specific suppression of a defective brassinosteroid receptor reveals a physiological role of UGGT in ER quality control. *Mol. Cell* **26**, 821-830. doi:10.1016/j.molcel.2007.05.015

Kanodia, P., Vijayapalani, P., Srivastava, R., Bi, R. and Howell, S. H. (2020). Control of translation during the unfolded protein response in maize seedlings: life without PERKs. *Plant Direct* **4**, e00241. doi:10.1002/pld3.241

Kim, T. W., Michniewicz, M., Bergmann, D. C. and Wang, Z. Y. (2012). Brassinosteroid regulates stomatal development by GSK3-mediated inhibition of a MAPK pathway. *Nature* **482**, 419-422. doi:10.1038/nature10794

Kubo, M., Udagawa, M., Nishikubo, N., Horiguchi, G., Yamaguchi, M., Ito, J., Mimura, T., Fukuda, H. and Demura, T. (2005). Transcription switches for protoxylem and metaxylem vessel formation. *Genes Dev.* **19**, 1855-1860. doi:10.1101/gad.1331305

Lampard, G. R., Macalister, C. A. and Bergmann, D. C. (2008). *Arabidopsis* stomatal initiation is controlled by MAPK-mediated regulation of the bHLH SPEECHLESS. *Science* **322**, 1113-1116. doi:10.1126/science.1162263

Lampard, G. R., Wengier, D. L. and Bergmann, D. C. (2014). Manipulation of mitogen-activated protein kinase kinase signaling in the *Arabidopsis* stomatal lineage reveals motifs that contribute to protein localization and signaling specificity. *Plant Cell* **26**, 3358-3371. doi:10.1105/tpc.114.127415

Langhans, M., Förster, S., Helmchen, G. and Robinson, D. G. (2011). Differential effects of the brefeldin A analogue (6R)-hydroxy-BFA in tobacco and *Arabidopsis*. *J. Exp. Bot.* **62**, 2949-2957. doi:10.1093/jxb/err007

Le, J., Liu, X. G., Yang, K. Z., Chen, X. L., Zou, J. J., Wang, H. Z., Wang, M., Vanneste, S., Morita, M., Tasaka, M. et al. (2014). Auxin transport and activity regulate stomatal patterning and development. *Nat. Commun.* **5**, 3090. doi:10.1038/ncomms4090

Leng, Y.-J., Yao, Y.-S., Yang, K.-Z., Wu, P.-X., Zuo, C.-R., Luo, J.-H., Wang, P., Liu, Y.-Y., Zhang, X.-Q., Ye, D. et al. (2022). *Arabidopsis* ERdj3B coordinates with ERECTA-family receptor kinases to regulate ovule development and the heat stress response. *Plant Cell* **28**, koac226. doi:10.1093/plcell/koac226

Maruyama, D., Sugiyama, T., Endo, T. and Nishikawa, S. (2014a). Multiple BiP genes of *Arabidopsis thaliana* are required for male gametogenesis and pollen competitiveness. *Plant Cell Physiol.* **55**, 801-810. doi:10.1093/pcp/pcu018

Maruyama, D., Yamamoto, M., Endo, T. and Nishikawa, S. (2014b). Different sets of ER-resident J-proteins regulate distinct polar nuclear-membrane fusion events in *Arabidopsis thaliana*. *Plant Cell Physiol.* **55**, 1937-1944. doi:10.1093/pcp/pcu120

Meng, X., Chen, X., Mang, H., Liu, C., Yu, X., Gao, X., Torii, K. U., He, P. and Shan, L. (2015). Differential function of *Arabidopsis* SERK family receptor-like kinases in stomatal patterning. *Curr. Biol.* **25**, 2361-2372. doi:10.1016/j.cub.2015.07.068

Nadeau, J. A. and Sack, F. D. (2002). Control of stomatal distribution on the *Arabidopsis* leaf surface. *Science* **296**, 1697-1700. doi:10.1126/science.1069596

Naramoto, S., Otegui, M. S., Kutsuna, N., de Rycke, R., Dainobu, T., Karampelias, M., Fujimoto, M., Feraru, E., Miki, D., Fukuda, H. et al. (2014). Insights into the localization and function of the membrane trafficking regulator GNOM ARF-GEF at the Golgi apparatus in *Arabidopsis*. *Plant Cell* **26**, 3062-3076. doi:10.1105/tpc.114.125880

Nekrasov, V., Li, J., Batoux, M., Roux, M., Chu, Z. H., Lacombe, S., Rougon, A., Bittel, P., Kiss-Papp, M., Chinchilla, D. et al. (2009). Control of the pattern-recognition receptor EFR by an ER protein complex in plant immunity. *EMBO J.* **28**, 3428-3438. doi:10.1038/emboj.2009.262

Olden, K., Parent, J. B. and White, S. L. (1982). Carbohydrate moieties of glycoproteins. A re-evaluation of their function. *Biochim. Biophys. Acta* **650**, 209-232. doi:10.1016/0304-4157(82)90017-x

Pillitteri, L. J. and Torii, K. U. (2012). Mechanisms of stomatal development. *Annu. Rev. Plant Biol.* **63**, 591-614. doi:10.1146/annurev-arplant-042811-105451

Qi, X., Yoshinari, A., Bai, P., Maes, M., Zeng, S. M. and Torii, K. U. (2020). The manifold actions of signaling peptides on subcellular dynamics of a receptor specify stomatal cell fate. *Elife* **9**, e58097. doi:10.7554/eLife.58097

Qu, X., Peterson, K. M. and Torii, K. U. (2017). Stomatal development in time: the past and the future. *Curr. Opin. Genet. Dev.* **45**, 1-9. doi:10.1016/j.gde.2017.02.001

Shpak, E. D., McAbee, J. M., Pillitteri, L. J. and Torii, K. U. (2005). Stomatal patterning and differentiation by synergistic interactions of receptor kinases. *Science* **309**, 290-293. doi:10.1126/science.1109710

Strasser, R. (2018). Protein quality control in the endoplasmic reticulum of plants. *Annu. Rev. Plant Biol.* **69**, 147-172. doi:10.1146/annurev-arplant-042817-040331

Sugano, S. S., Shimada, T., Imai, Y., Okawa, K., Tamai, A., Mori, M. and Hara-Nishimura, I. (2010). Stomagen positively regulates stomatal density in *Arabidopsis*. *Nature* **463**, 241-244. doi:10.1038/nature08682

Swarup, R., Kargul, J., Marchant, A., Zadik, D., Rahman, A., Mills, R., Yemm, A., May, S., Williams, L., Millner, P. et al. (2004). Structure-function analysis of the presumptive *Arabidopsis* auxin permease AUX1. *Plant Cell* **16**, 3069-3083. doi:10.1105/tpc.104.024737

Torii, K. U. (2012). Mix-and-match: ligand-receptor pairs in stomatal development and beyond. *Trends Plant Sci.* **17**, 711-719. doi:10.1016/j.tplants.2012.06.013

Yamamoto, M., Maruyama, D., Endo, T. and Nishikawa, S. (2008). *Arabidopsis thaliana* has a set of J proteins in the endoplasmic reticulum that are conserved from yeast to animals and plants. *Plant Cell Physiol.* **49**, 1547-1562. doi:10.1093/pcp/pcn119

Yamamoto, M., Uji, S., Sugiyama, T., Sakamoto, T., Kimura, S., Endo, T. and Nishikawa, S. I. (2020). ERdj3B-Mediated quality control maintains anther development at high temperatures. *Plant Physiol.* **182**, 1979-1990. doi:10.1104/pp.19.01356

Yang, M. and Sack, F. D. (1995). The too many mouths and four lips mutations affect stomatal production in *Arabidopsis*. *Plant Cell* **7**, 2227-2239. doi:10.1105/tpc.7.12.2227

Yang, K. Z., Xia, C., Liu, X. L., Dou, X. Y., Wang, W., Chen, L. Q., Zhang, X. Q., Xie, L. F., He, L., Ma, X. et al. (2009). A mutation in *Thermosensitive Male Sterile 1*, encoding a heat shock protein with DnaJ and PDI domains, leads to thermosensitive gametophytic male sterility in *Arabidopsis*. *Plant J.* **57**, 870-882. doi:10.1111/j.1365-313X.2008.03732.x

Zhang, Y., Wang, P., Shao, W., Zhu, J. K. and Dong, J. (2015). The BASL polarity protein controls a MAPK signaling feedback loop in asymmetric cell division. *Dev. Cell* **33**, 136-149. doi:10.1016/j.devcel.2015.02.022

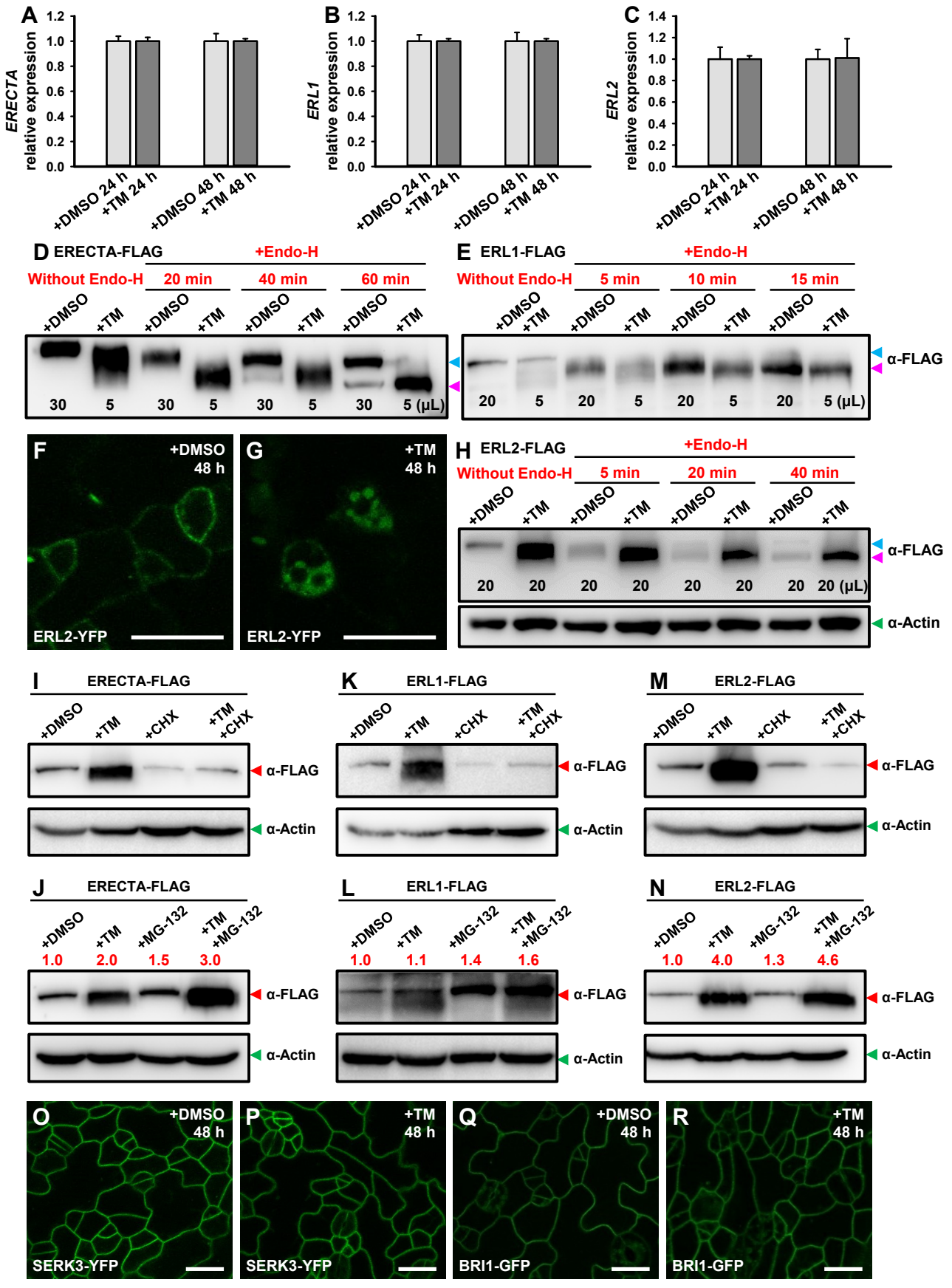

Fig. S1. Endo-H assay of ERECTA-family proteins and ERL2-YFP expression after TM treatment.

(A-C) RT-qPCR analysis of the transcript levels of ERECTA-family genes. No significant differences are found between mock (DMSO) and TM treatments. Data are mean±s.d. of three biological replicates. (D) Immunoblotting analysis of ERECTA-FLAG extracted from mock and TM-treated plants with and without Endo-H digestion. ERECTA-FLAG from TM-treated plants was sensitive to Endo-H digestion, showing a stronger lower band (cleaved proteins) in immunoblot after Endo-H digestion (pink arrowhead). Prolonged Endo-H digestion of 40 min or 60 min produced two bands in control plants. While, the upper band (non-cleaved proteins) was faint in TM-treated plants (blue arrowhead). The samples without Endo-H digestion are presented as control (left two lanes). Notice the fast moving of ERECTA-FLAG protein from the TM-treated plants. (E) Immunoblotting analysis of ERL1-FLAG protein after Endo-H digestion. ERL1-FLAG from TM-treated plants was sensitive to Endo-H digestion, showing a faster mobility in immunoblot. (F, G) Confocal images of *ERL2:ERL2-YFP* epidermis. Strong intracellular ERL2-YFP signals were detected in the stomatal precursor cells after TM treatment. (H) Immunoblotting analysis of ERL2-FLAG with and without Endo-H digestion. In contrast to the two bands of ERL2-FLAG in control plants (blue and pink arrowheads), Endo-H digestion of ERL2-FLAG protein from TM-treated plants resulted in a single band with faster mobility. Lower panel, the loading control of actin detected by anti-Actin (green arrowhead). (I-N) Immunoblotting analysis of ERECTA-FLAG, ERL1-FLAG and ERL2-FLAG extracted from mock and treated with TM, CHX, TM with CHX, MG-132, and TM with MG-132. Top panel, the ERECTA-family protein bands detected by anti-FLAG (red arrowhead). Lower panel, the loading control of actin detected by anti-Actin (green arrowhead). The red numbers above the upper panel are relative ratios of mean gray values of bands to the DMSO control. (O-R) No obvious changes of SERK3-YFP and BRI1-GFP in epidermis were observed after TM treatment. Images are representative of three independent experiments.
Scale bars: 20 μm.

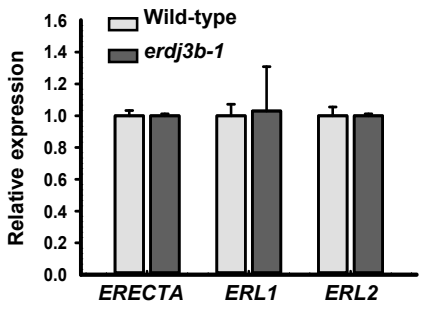

Fig. S2. RT-qPCR analysis of the transcript levels of ERECTA-family genes. No significant differences were found between wild-type and *erdj3b-1* mutant. Data are mean±s.d. of three biological replicates.

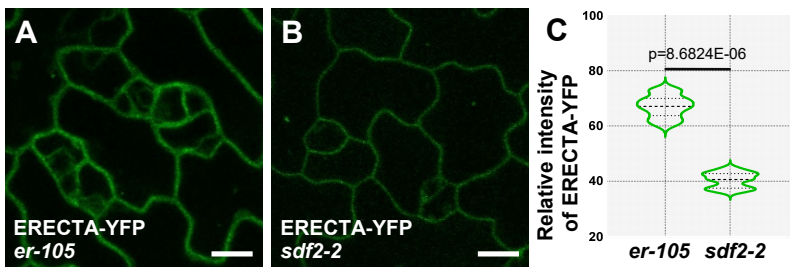

Fig. S3. The overall fluorescence intensity of ERECTA-YFP is reduced in *sdf2-2* mutant. (A, B) Confocal images of ERECTA-YFP in *er-105* (complementary) and *sdf2-2* mutant leaf epidermis. Scale bars: 20 μm. (C) Quantification fluorescence intensity in stomatal precursor cells. ERECTA-YFP intensity in *er-105* is statistically different from that in *sdf2- 2* after two-tailed unpaired Student's *t*-test (*n*=21). Dotted lines indicate the 25th-75th percentiles and dashed lines indicate the median.

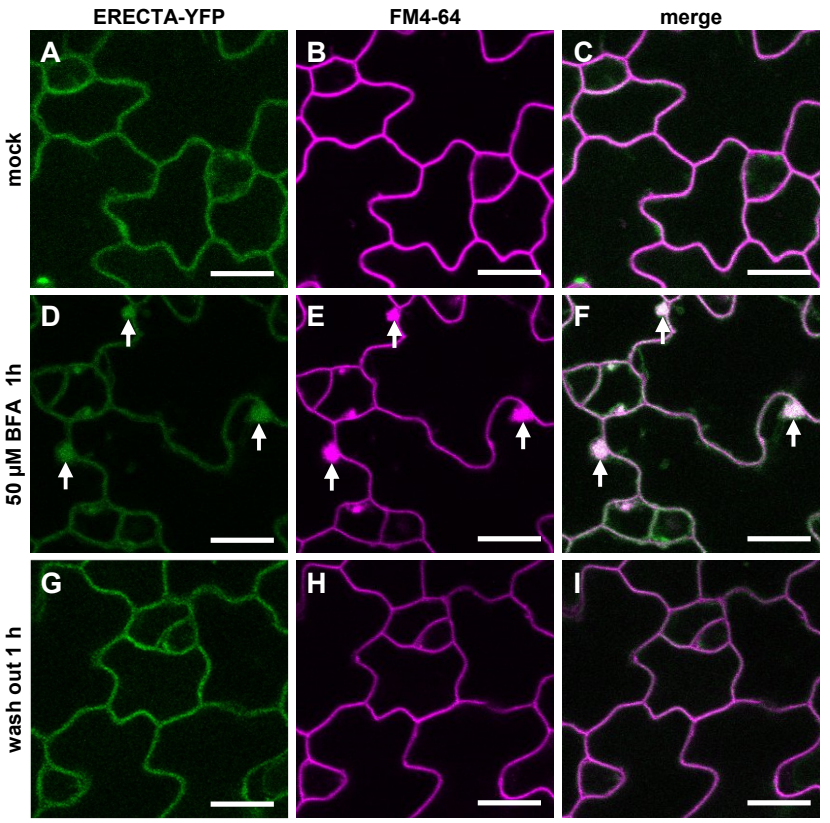

Fig. S4. Effects of BFA on subcellular localization of ERECTA-YFP.
(A-C) Confocal images show the colocalization of ERECTA-YFP (*er-105* complementary) with FM4-64 at the PM. (D-F) Confocal images show the aggregation of ERECTA-YFP and FM4- 64 in BFA-bodies (white arrows) at 1 h after 50 µM BFA treatment. (G-I) Confocal images show the colocalization of ERECTA-YFP colocalizes with FM4-64 at the PM in BFA-treated plants after 1 h water rinse (wash out).
Scale bars: 20 µm.

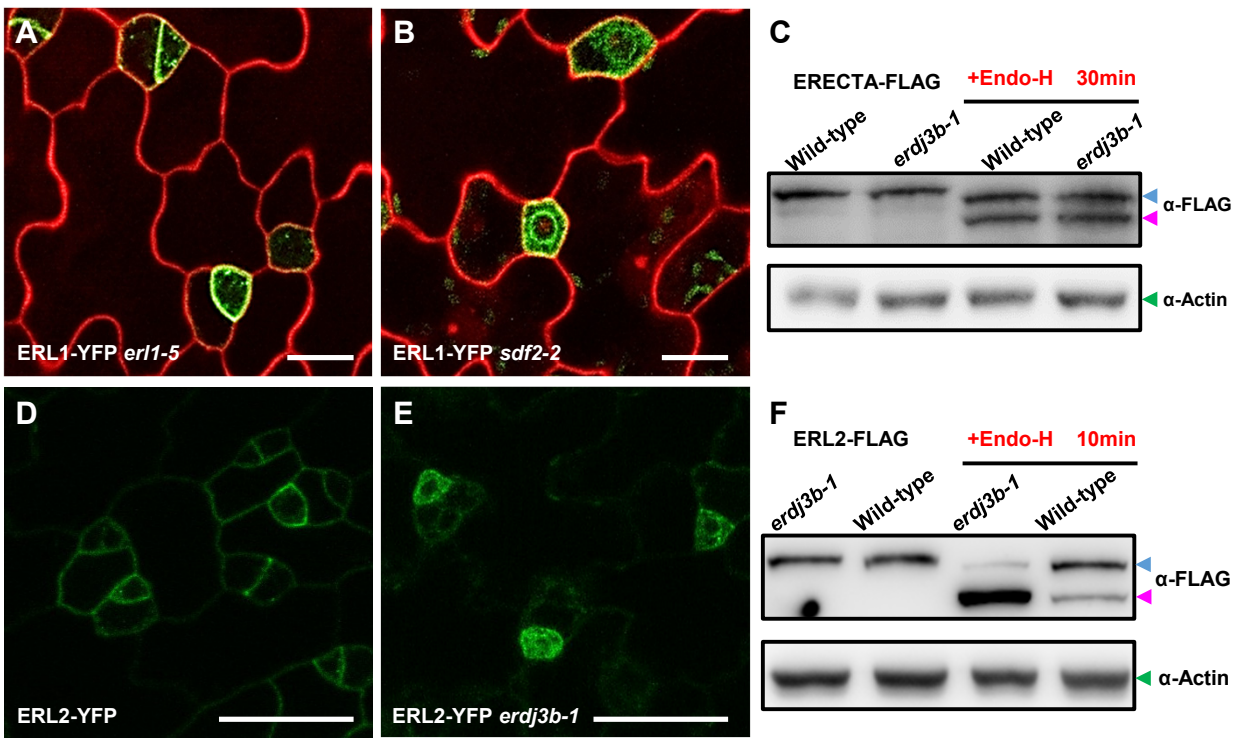

Fig. S5. Dysfunction of SDF2-ERdj3B-BiP complex causes retention of ERL1 and ERL2 in the ER. (A, B) ERL1-YFP (*erl1-5* complementary) predominantly localizes at the PM in stomatal precursor cells. In *sdf2-2*, ERL1-YFP is present in ring-like structure. Cell outlines are visualized with propidium iodide. (C) Immunoblot analysis of ERECTA-FLAG after Endo-H digestion. ERECTA-FLAG proteins extracted from wild-type and *erdj3b-1* plants show a similar response to Endo-H digestion. A blue and a pink arrowhead indicate the non-cleaved proteins (upper band) and cleaved proteins (lower band), respectively. Lower panel, loading control of actin detected by anti-Actin. (D, E) ERL2-YFP predominantly resides at the PM of stomatal precursor cells in the wild-type plants. In *erdj3b-1,* strong ERL2-YFP signals are detected in the ring-like structure. (F) Immunoblot analysis of ERL2 after Endo-H digestion. ERL2-FLAG protein extracted from *erdj3b-1* plants are sensitive to Endo-H digestion, comparing with ERL2-FLAG in wild-type plants, showing a stronger lower band (cleaved proteins) in immunoblot analysis. Images are representative of three independent experiments.
Scale bars: 20 μm.

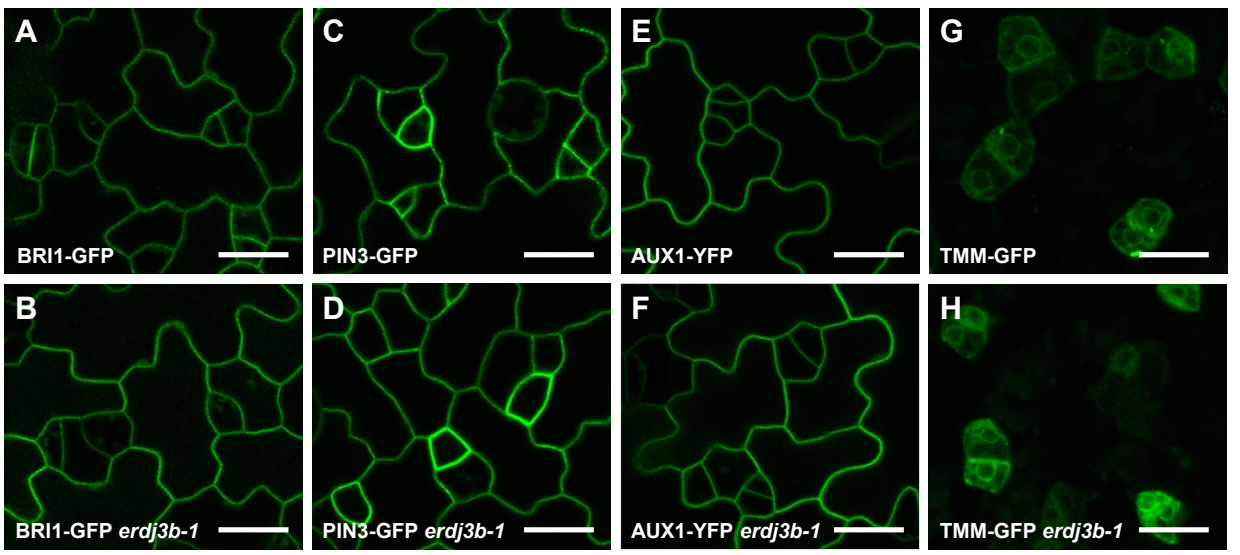

Fig. S6. BRI1-GFP, PIN3-GFP, AUX1-YFP and TMM-GFP expression in wild-type and *erdj3b-1* epidermis.

No obvious changes of BRI1-GFP, PIN3-GFP, AUX1-YFP, and TMM-GFP expression and localization were found in *erdj3b-1* mutant epidermis, comparing that in wild-type background.

Scale bars: 20 μm.

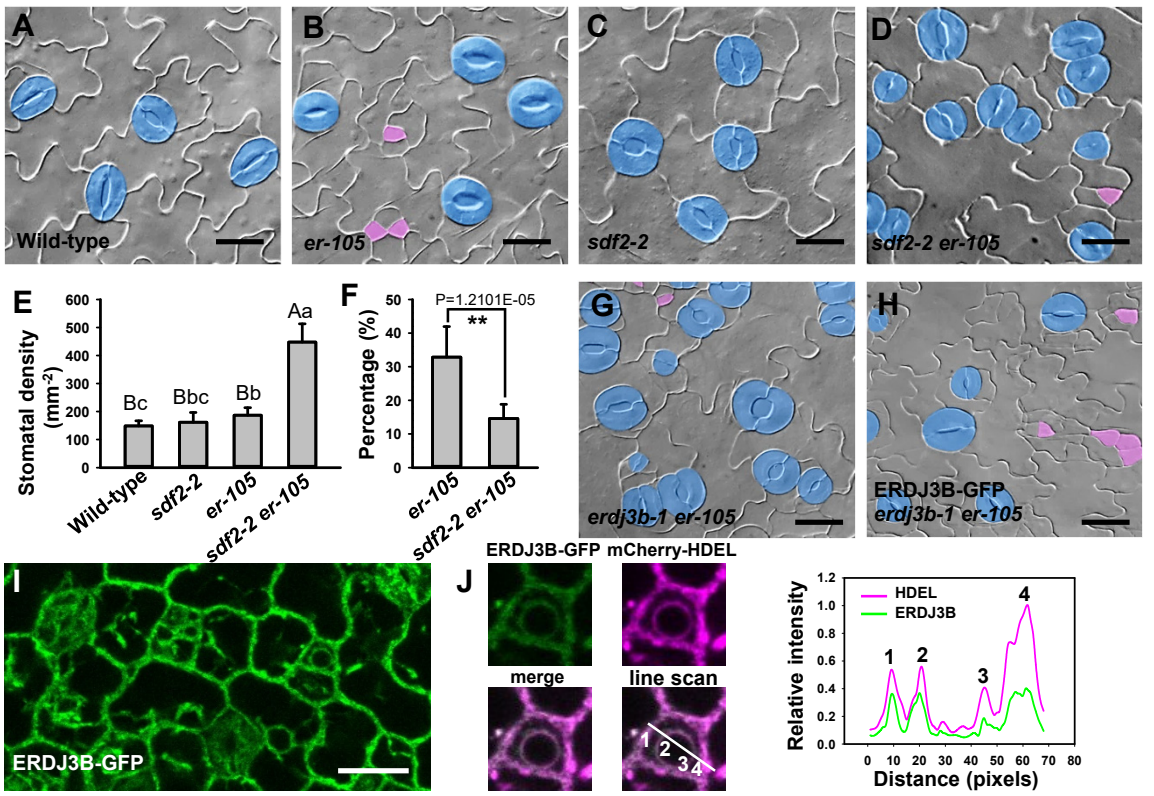

Fig. S7. ER-resident SDF2-ERdj3B-BiP is differentially involved in stomatal development regulation.

(A-D) DIC images of epidermis of 12-day-old cotyledons. Mature stomata are highlighted by blue color. Precursor-like Cells (PrCs) are highlighted by pink color. Mutation of *sdf2* promotes the differentiation of PrCs in *er-105* into mature stomata, leading to an increase of stomatal production and stomatal clusters. (E) Quantitative analysis of stomatal density. Values are mean±s.d. (*n*=18). Data were analyzed using one-way ANOVA with Tukey's post hoc test. The different uppercase and lowercase letters indicate significant differences at 1% and 5%, respectively. (F) Quantification of the percentage of PrCs over total number of PrCs and mature stomata. Values are mean±s.d.. Asterisks indicate significant difference after two-tailed unpaired Student's *t*-test, ***P*<0.01. (G, H) Introduction of *ERDJ3B:ERDJ3B-GFP* restored the appearance of arrested precursor cells in *erdj3b-1 er-105*, resembling the stomatal phenotype in *er-105* single mutant. (I) Confocal image of *ERDJ3B:ERDJ3B-GFP* expression in epidermis cells. (J) Quantitative analysis of fluorescence intensity profiles revealed the colocalization of ERDJ3B-GFP with mCherry-HDEL in the ER.
Scale bars: 20 μm.

Table S1. Nucleotide sequences of primer sets used in this study.

Click here to download Table S1